Chemistry–A European Journal

Supporting Information

# A Multiresponsive Calix[6]arene Pseudorotaxane Empowered by Fluorophoric Dansyl Groups

Leonardo Andreoni, Giovanni Mariano Beneventi, Gabriele Giovanardi, Gianpiero Cera,*
Alberto Credi, Arturo Arduini, Andrea Secchi,* and Serena Silvi*

## Table of Contents

- **Synthesis of TDA and NMR Characterisation**

In a two-necked round-bottomed flask, under $N_2$ atmosphere, Pd/C (10 mol %) was added to a suspension of **TN** (0.3 mmol) in EtOH (200 ml). Subsequently, $NH_2NH_2 \bullet H_2O$ (6 mmol, 20 eq.) was added dropwise, and the reaction placed in an oil-bath where it was refluxed for 24 h. After completion, determined by TLC analysis, the reaction was cooled down to room temperature, and then filtered through a Celite pad to remove the Pd/C catalyst. The mixture was concentrated at reduced pressure and water (30 ml) was added. After extraction with $CH_2Cl_2$ (3 × 30 ml), organic phases were dried over $Na_2SO_4$ and concentrated at reduced pressure to afford a pale-yellow solid. The crude was dissolved with dry $CH_2Cl_2$ (20 ml) under $N_2$ atmosphere and triethylamine (1.5 mmol, 5.0 eq.) was added. Subsequently, 5-dimethylaminonaphthalene-1-sulphonyl chloride (1.2 mmol, 4.0 eq.) was added at 0 °C. The reaction was stirred for 4 h. After completion, a solution of sat. $NH_4Cl$ (20 ml) was added, and the mixture extracted with $CH_2Cl_2$ (3 × 30 ml). The joined organic layers were dried over $Na_2SO_4$, concentrated at reduced pressure and the crude purified by column chromatography on silica gel (n-Hex/AcOEt: 80:20) affording **TDA** (447mg, 77%) as a yellow solid. M. p. = 128-130 °C. $^1$H NMR (400 MHz, $CD_2Cl_2$) $\delta$ = 8.57 (d, *J* = 8.3 Hz, 3H), 8.28 (d, *J* = 8.6 Hz, 3H), 8.08 (d, *J* = 7.3 Hz, 3H), 7.54 – 7.50 (m, 3H), 7.50 – 7.44 (m, 3H), 7.21 (d, *J* = 7.6 Hz, 3H), 7.12 (s, 6H), 6.27 (s, 6H), 4.31 (d, *J* = 15.4 Hz, 6H), 3.82 (t, *J* = 6.6 Hz, 6H), 3.34 (d, *J* = 15.4 Hz, 6H), 2.93 (s, 18H), 2.57 (s, 9H), 1.95 – 1.76 (m, 6H), 1.63 – 1.51 (m, 6H), 1.44 – 1.26 (m, 51H), 0.90 (t, *J* = 6.8 Hz, 9H). $^{13}$C NMR (101 MHz, $CD_2Cl_2$) $\delta$ = 154.5 ($C_q$), 151.8 ($C_q$), 151.2 ($C_q$), 146.3 ($C_q$), 135.7 (2x$C_q$), 134.2 ($C_q$), 132.9 ($C_q$), 132.1 ($C_q$), 130.6 (CH), 130.4 (CH), 129.7 ($C_q$), 128.4 (CH), 127.7 (CH), 122.8 (CH), 119.1 (2xCH), 115.1 (CH), 73.0 ($CH_2$), 60.0 ($CH_3$), 45.2 ($CH_3$), 34.0 ($C_q$), 31.9 ($CH_2$), 31.4 ($CH_3$), 30.5 ($CH_2$), 30.4 ($CH_2$), 29.6 ($CH_2$), 29.3 ($CH_2$), 26.2 ($CH_2$), 22.7 ($CH_2$), 13.9 ($CH_3$). HR-MS: *m/z* $[M+H]^+$ calcd. for $C_{117}H_{151}N_6O_{12}S_3$: 1928.0552; found: 1928.0557. Elemental analysis calculated for $C_{117}H_{150}N_6O_{12}S_3$: C 72.86, H 7.84, N 4.36, S 4.99 found: C 72.48, H 7.81, N 4.25, S 4.82.

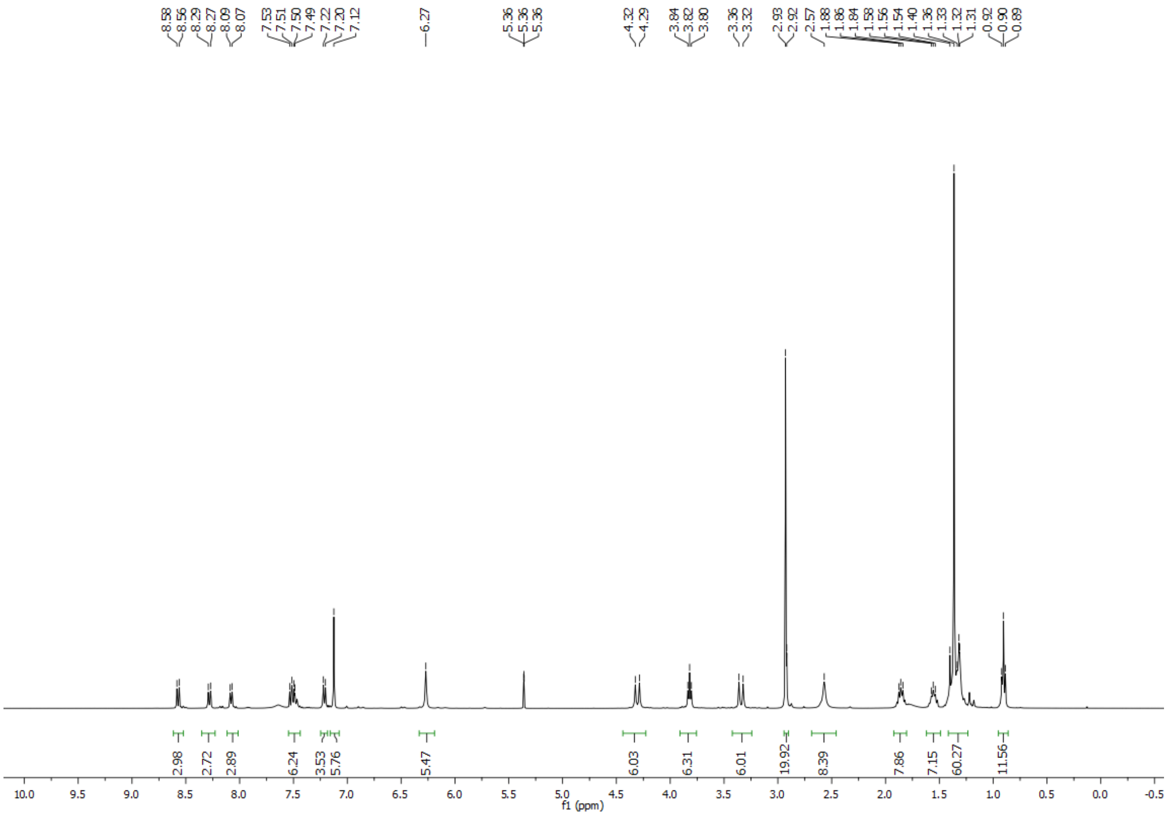

**Figure S1.** $^{1}$H-NMR ($CD_2Cl_2$, 400 MHz) of **TDA**.

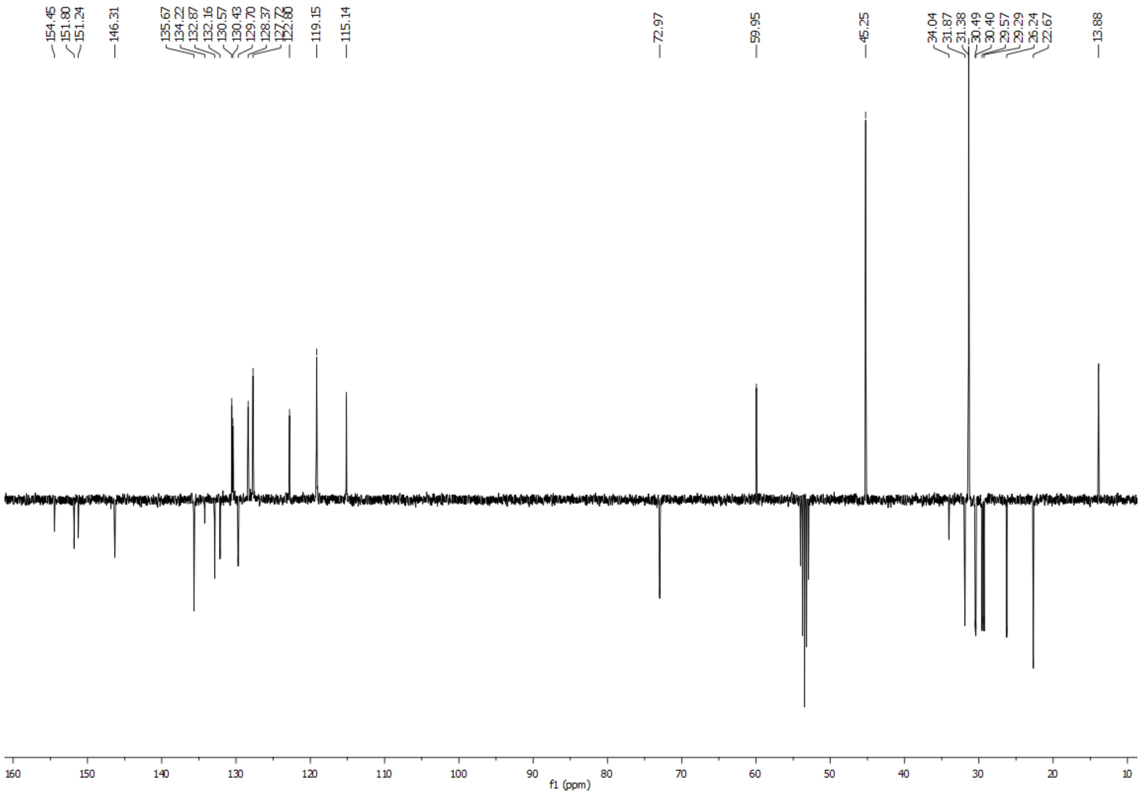

**Figure S2.** $^{13}$C-NMR DEPTQ ($CD_2Cl_2$, 101 MHz) of **TDA**.

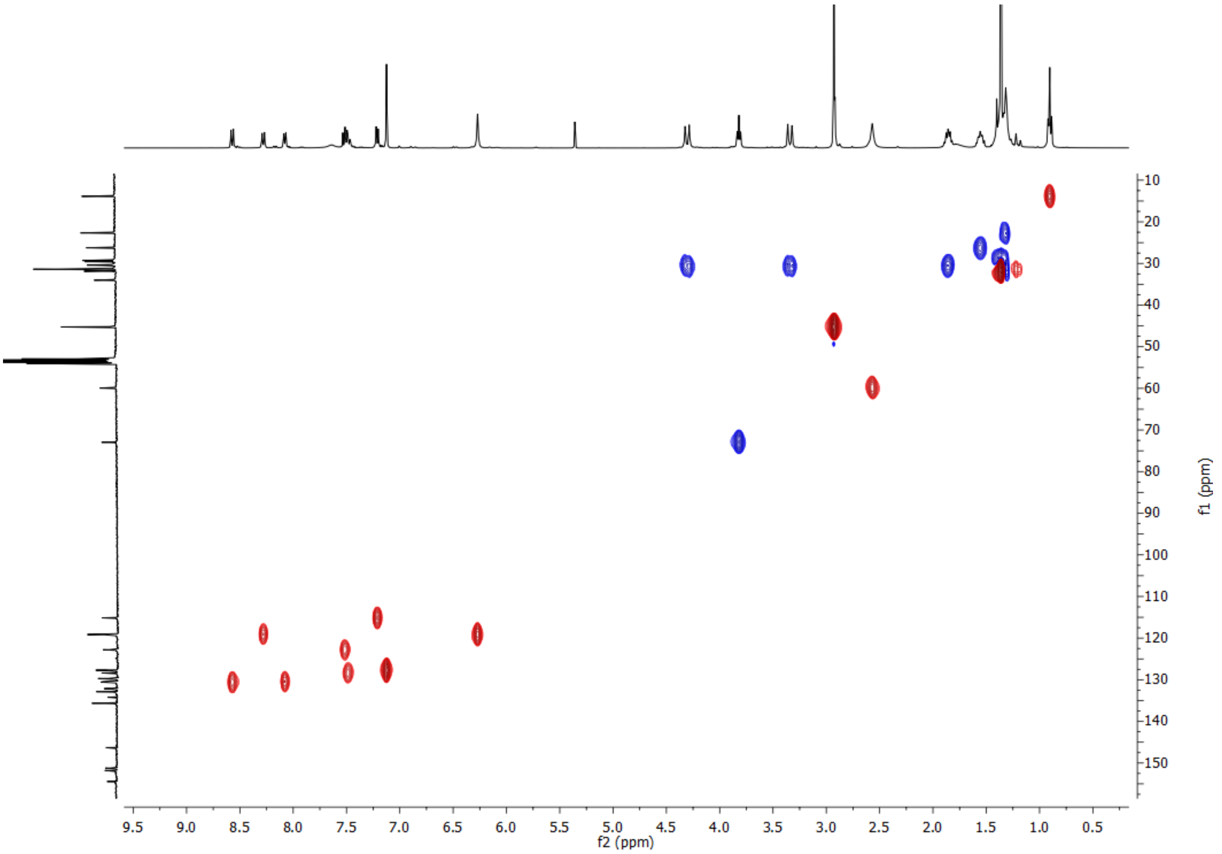

**Figure S3.** ge-2D multiplicity-edited ($CD_2Cl_2$, 400 MHz) NMR spectrum of **TDA**.

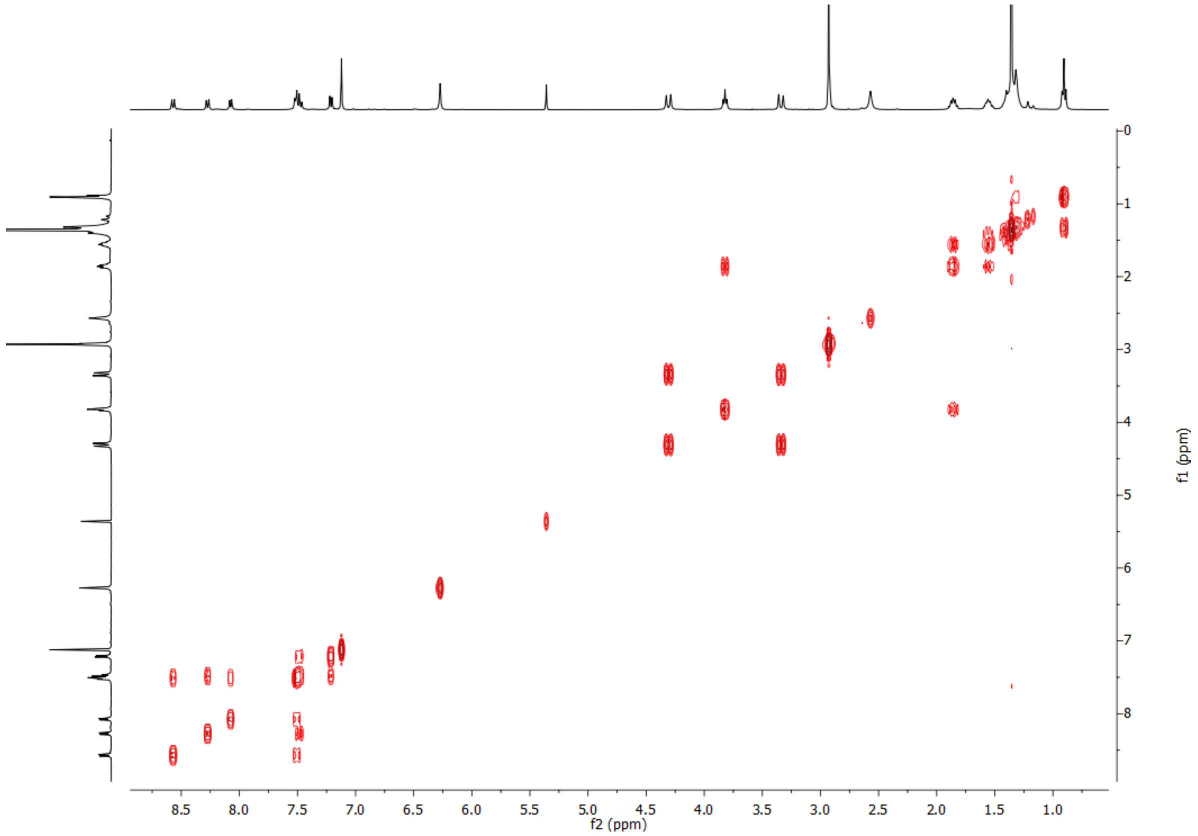

**Figure S4.** ge-2D COSY ($CD_2Cl_2$, 400 MHz) NMR spectrum of **TDA**.

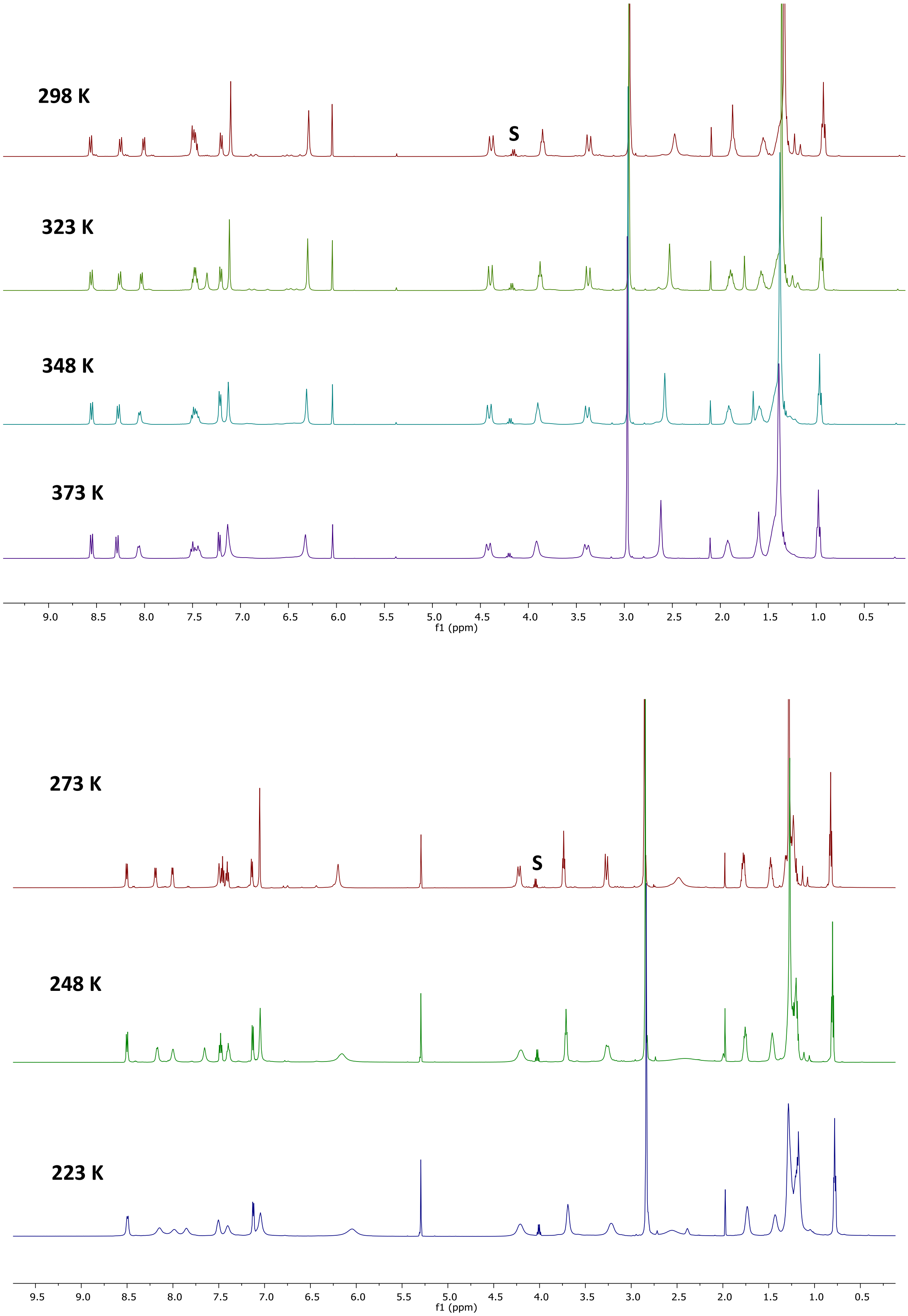

**Figure S5.** Stack plot of the $^1$H-NMR (1,1,2,2-tetrachloroethane-$d_2$, 400 MHz, TOP and $CD_2Cl_2$, 600 MHz, BOTTOM) spectra of **TDA** at different temperatures.

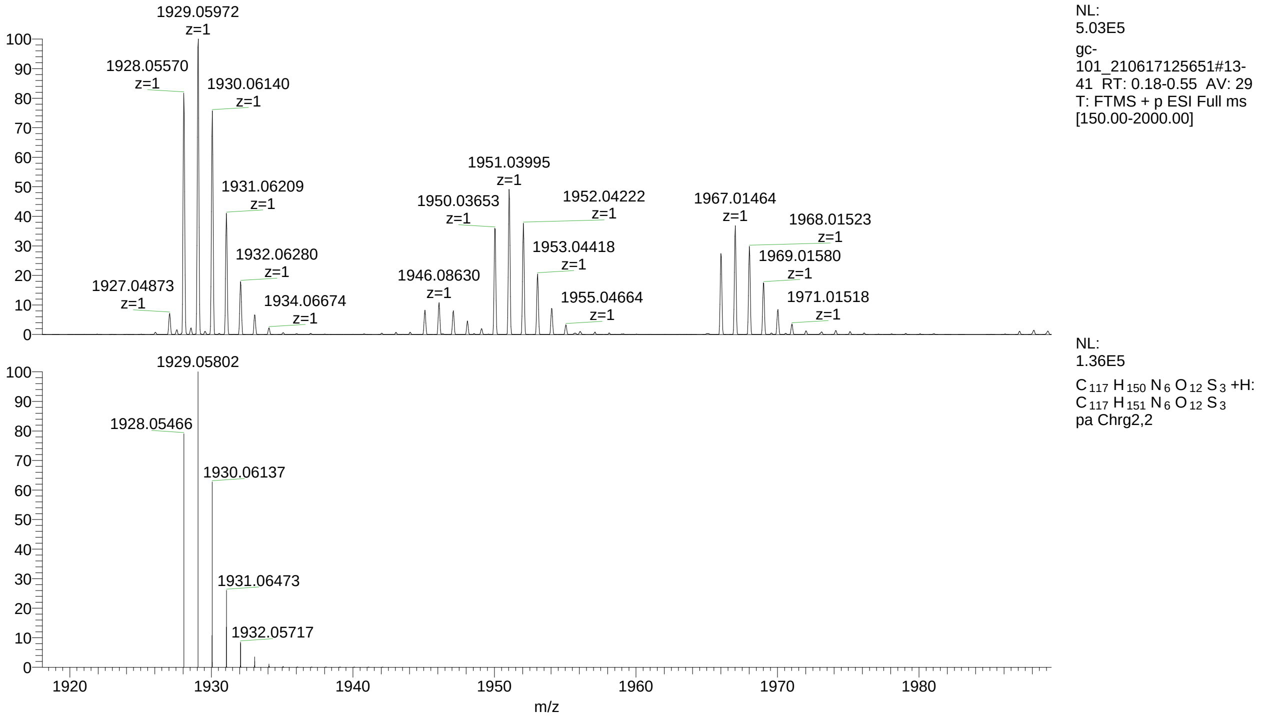

**Figure S6.** Experimental and simulated isotopic pattern of the molecular ion $[M+H]^+$ of **TDA**.

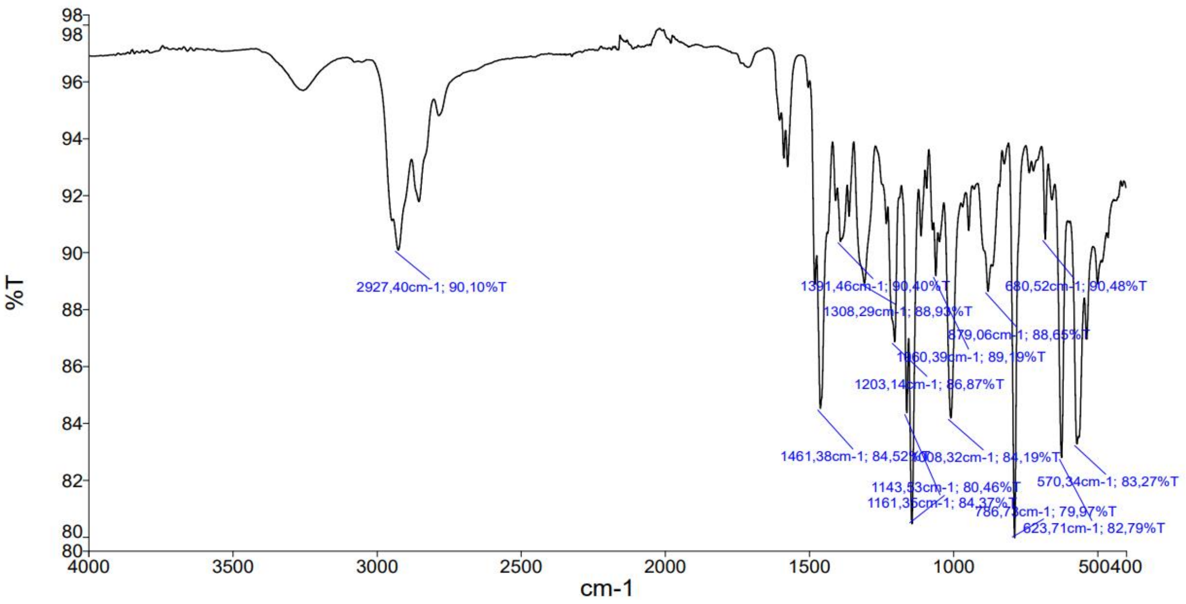

PerkinElmer Spectrum IR Version 10.6.1
martedì 10 gennaio 2023 12:20

List of Peak Area/Height

| Peak Number | X (cm-1) | Y (%T) |
|---|---|---|
| 1 | 2927,40 | 90,10 |
| 2 | 1461,38 | 84,52 |
| 3 | 1391,46 | 90,40 |
| 4 | 1308,29 | 88,93 |
| 5 | 1203,14 | 86,87 |
| 6 | 1161,35 | 84,37 |
| 7 | 1143,53 | 80,46 |
| 8 | 1060,39 | 89,19 |
| 9 | 1008,32 | 84,19 |
| 10 | 879,06 | 88,65 |
| 11 | 786,73 | 79,97 |
| 12 | 680,52 | 90,48 |
| 13 | 623,71 | 82,79 |
| 14 | 570,34 | 83,27 |

**Figure S7.** IR analysis (ATR) of **TDA**.

- **NMR Characterisation of Pseudorotaxane Species**

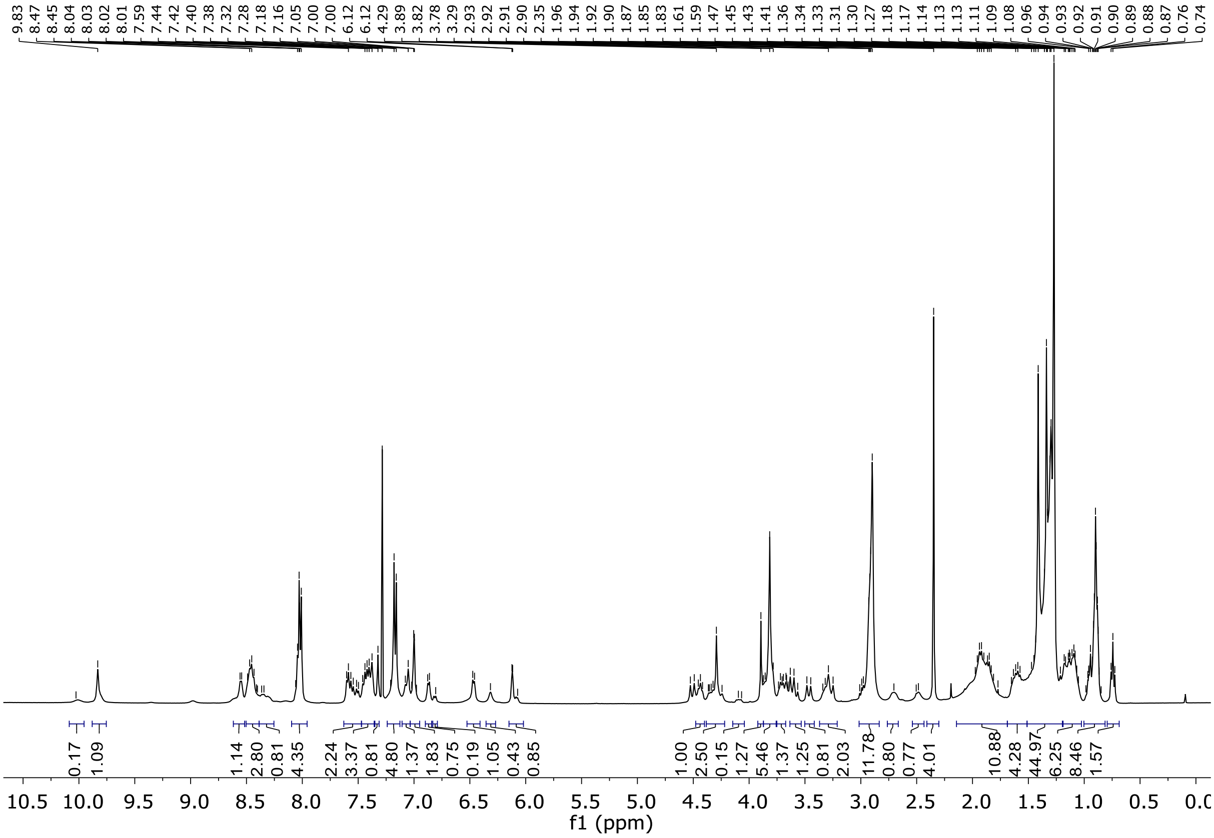

**Figure S8.** $^1$H-NMR ($CDCl_3$, 400 MHz) spectrum of P[**TDA**(p*C*)⊃DOV]2OTs.

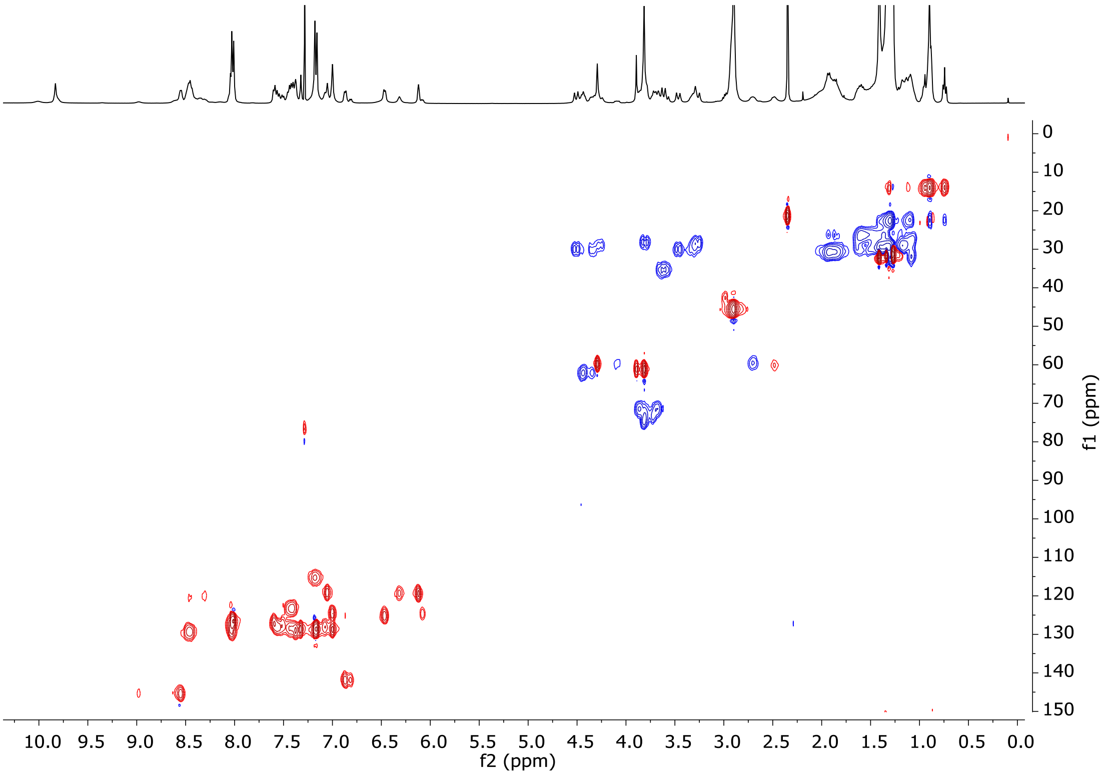

**Figure S9.** ge-2D multiplicity-edited ($CDCl_3$, 400 MHz) NMR spectrum of P[**TDA** (p*C*)⊃DOV]2OTs. Red contours cross-peaks show $CH_3$, CH correlations while the blue contours show $CH_2$ correlations.

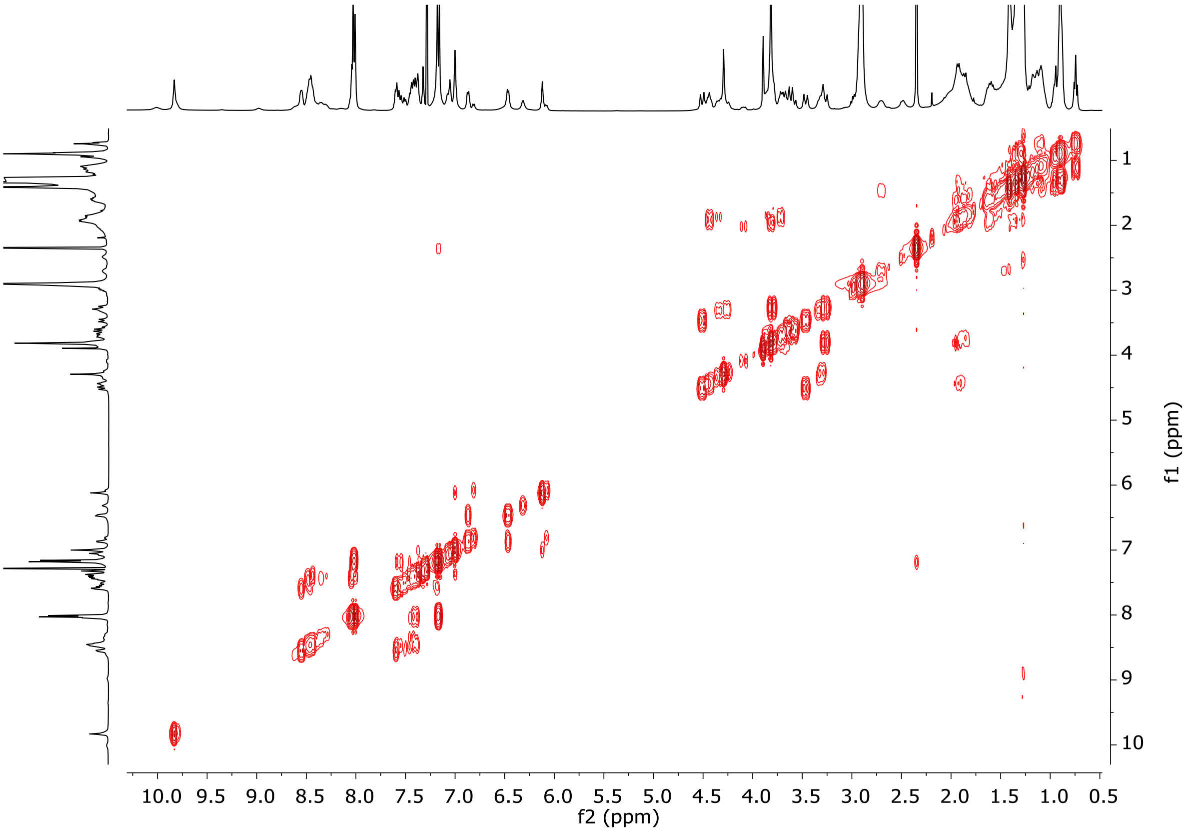

**Figure S10.** ge-2D COSY ($CDCl_3$, 400 MHz) NMR spectrum of P[**TDA**(p*C*)⊃DOV]2OTs.

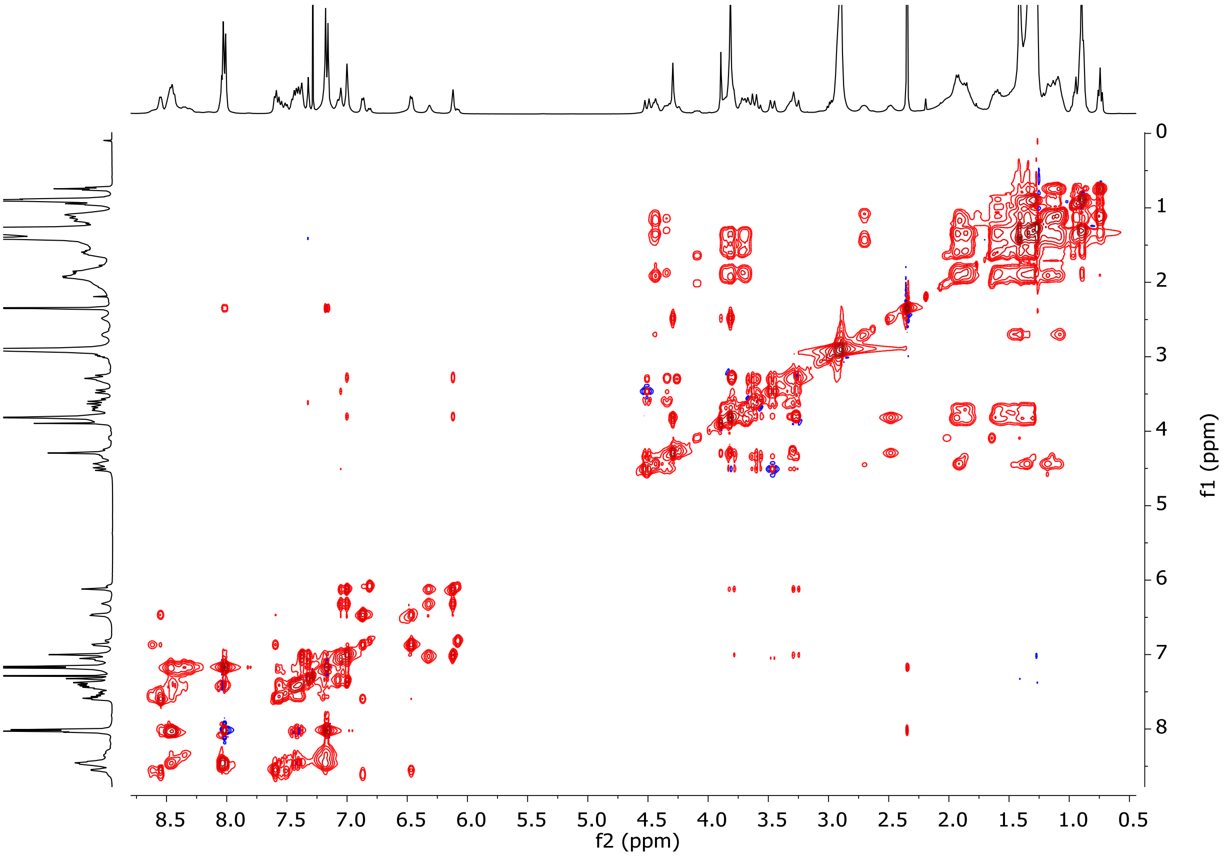

**Figure S11.** ge-2D TOCOSY ($CDCl_3$, 400 MHz) NMR spectrum of P[**TDA**(p*C*)⊃DOV]2OTs.

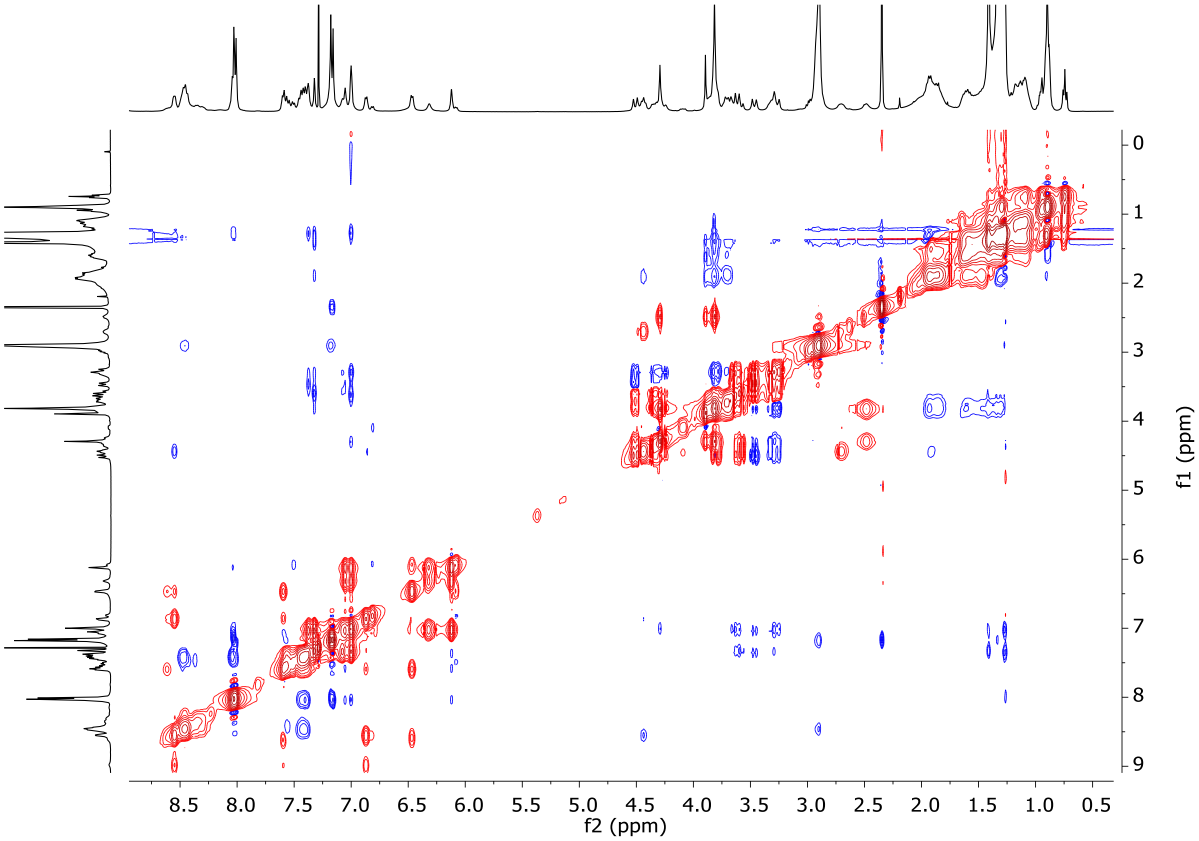

**Figure S12.** 2D ROESY ($CDCl_3$, 400 MHz) NMR spectrum of P[**TDA**(p*C*)⊃DOV]2OTs (spin-locking = 200 ms).

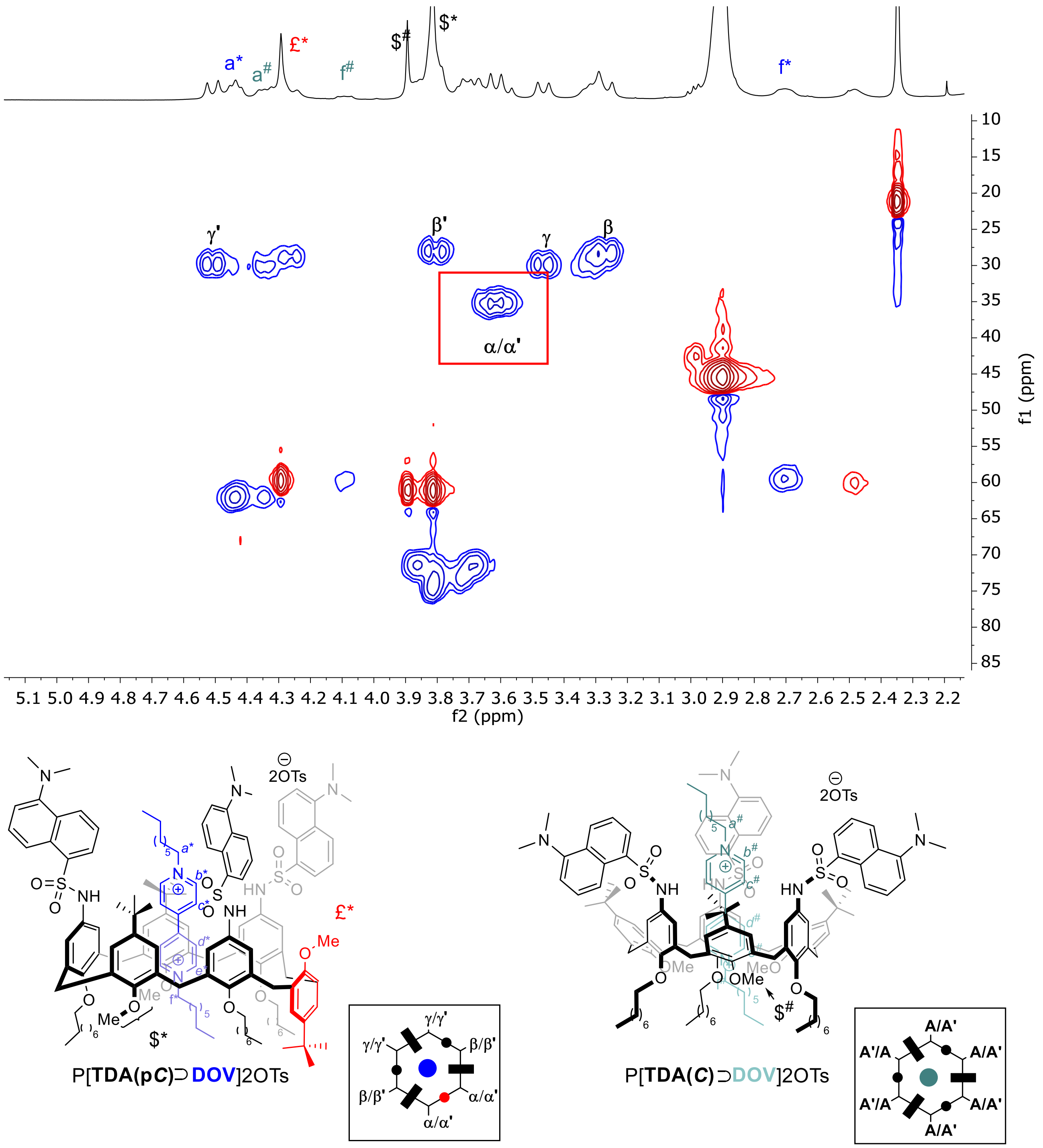

P[**TDA(p*C*)**⊃**DOV**]2OTs

P[**TDA(*C*)**⊃**DOV**]2OTs

**Figure S13**. Mid-field expanded region of the 2D HSQC NMR ($CDCl_3$, 400 MHz) spectrum of P[**TDA**(p*C*)⊃DOV]2OTs showing the downfield shift of $^{13}$C-NMR resonances of methylene protons due to a partial-cone (p*C*) conformation. In the red square, the correlation between the chemical shift of α/α′ protons and its carbons has been evidenced.

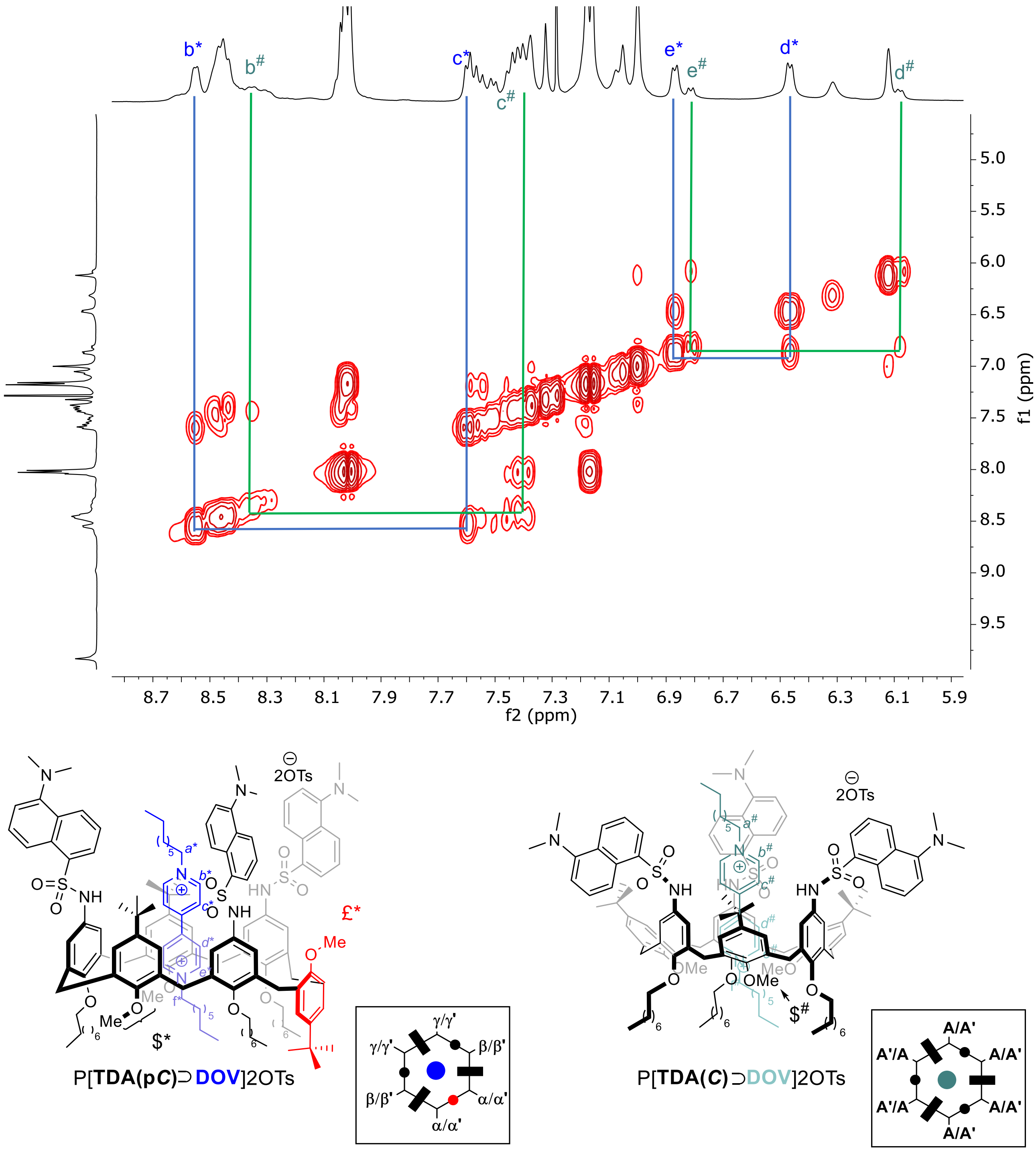

**Figure S14.** Low-field expanded region of the 2D $^{1}$H-$^{1}$H COSY NMR ($CDCl_3$, 400 MHz) spectrum of P[**TDA**(p*C*)⊃DOV]2OTs showing the J-coupling correlations between the aromatic protons of the threaded bipyridinium guest (DOV).

- **NMR Characterisation of the Protonated Pseudorotaxane Species**

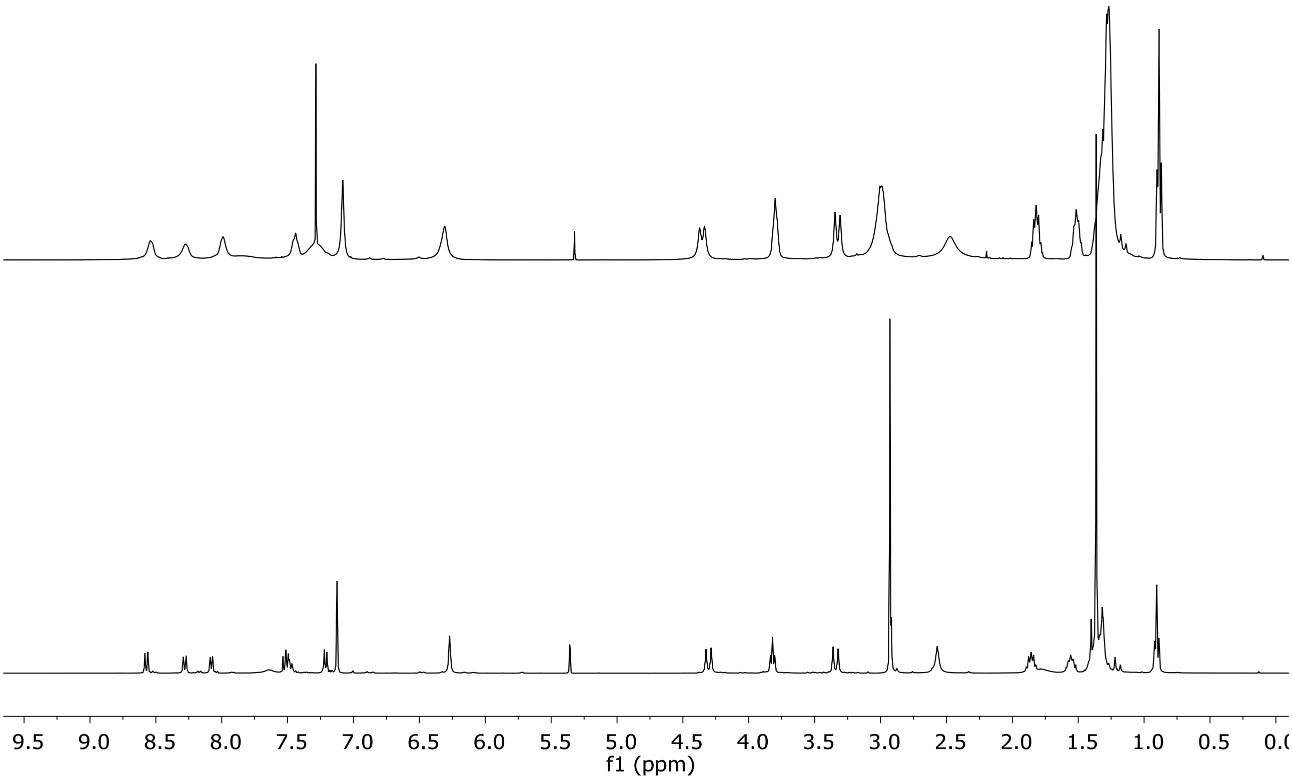

**Figure S15.** Stack plot of the 1H-NMR spectra of **TDA**(3H)3OTf ($CDCl_3$, 400 MHz, top) and **TDA** ($CD_2Cl_2$, 400 MHz) at 298 K.

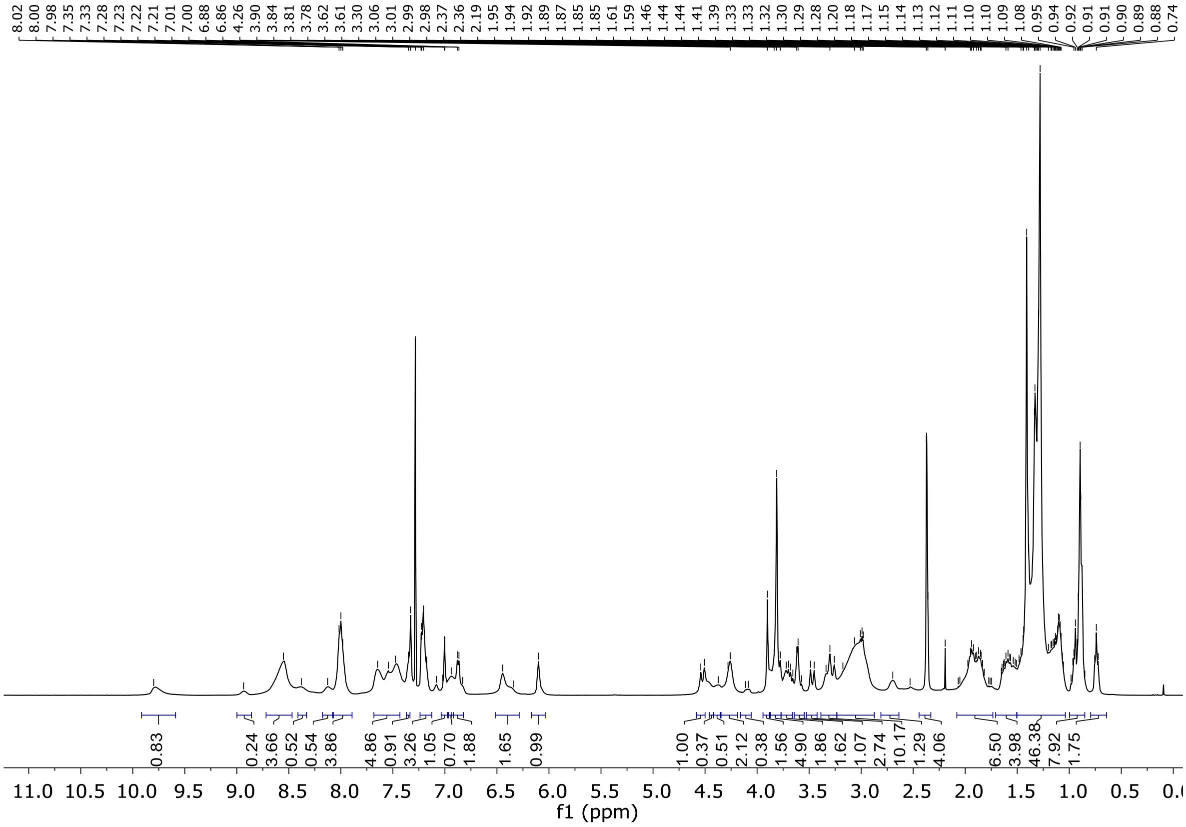

**Figure S16.** $^1$H-NMR ($CDCl_3$, 400 MHz) spectrum of P[**TDA**(3H)(p*C*)⊃DOV]2OTs(3OTf).

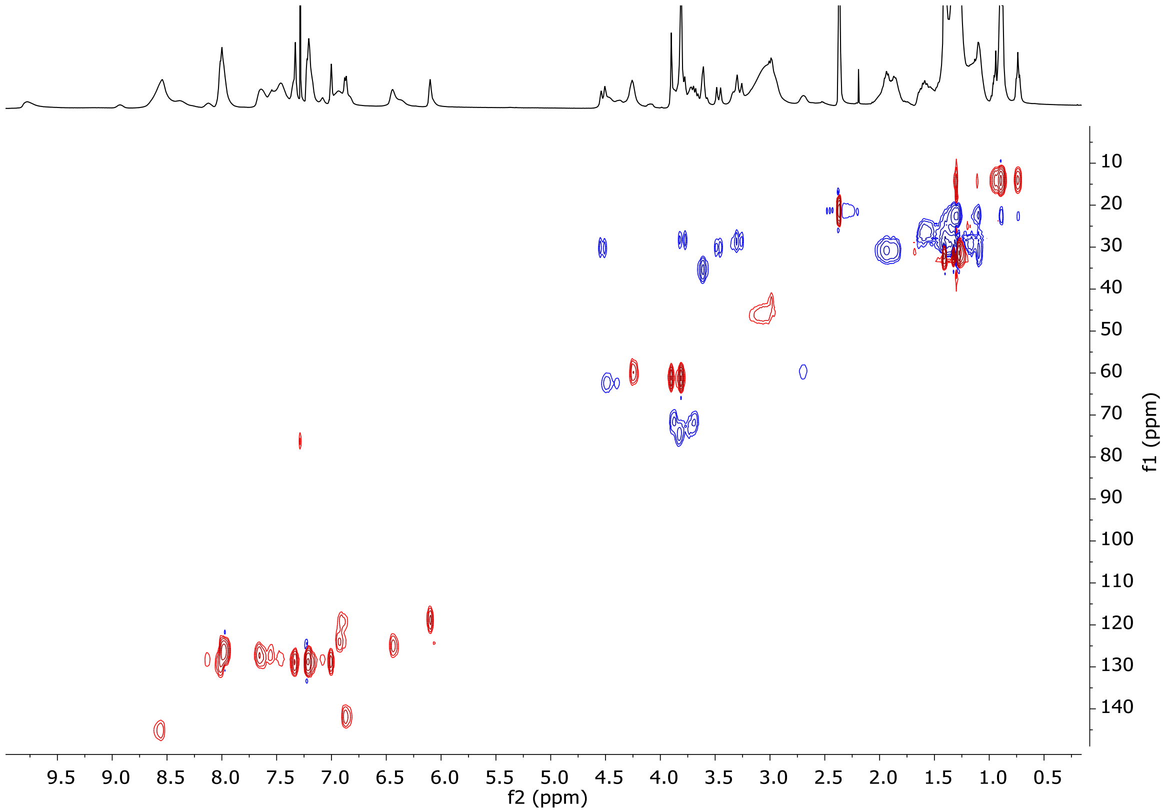

**Figure S17.** ge-2D multiplicity-edited ($CDCl_3$, 400 MHz) NMR spectrum of P[**TDA**(3H)(p*C*)⊃DOV]2OTs(3OTf). Red contours cross-peaks show $CH_3$, CH correlations while the blue contours show $CH_2$ correlations.

*Temperature effect on the conformation of pseudorotaxane complex P[**TDA**(3H)(pC)⊐DOV]2OTs(3OTf) obtained adding 3 equiv. of TfOH on a 5mM solution of P[**TDA**(3H)(pC)⊐DOV]2OTs.*

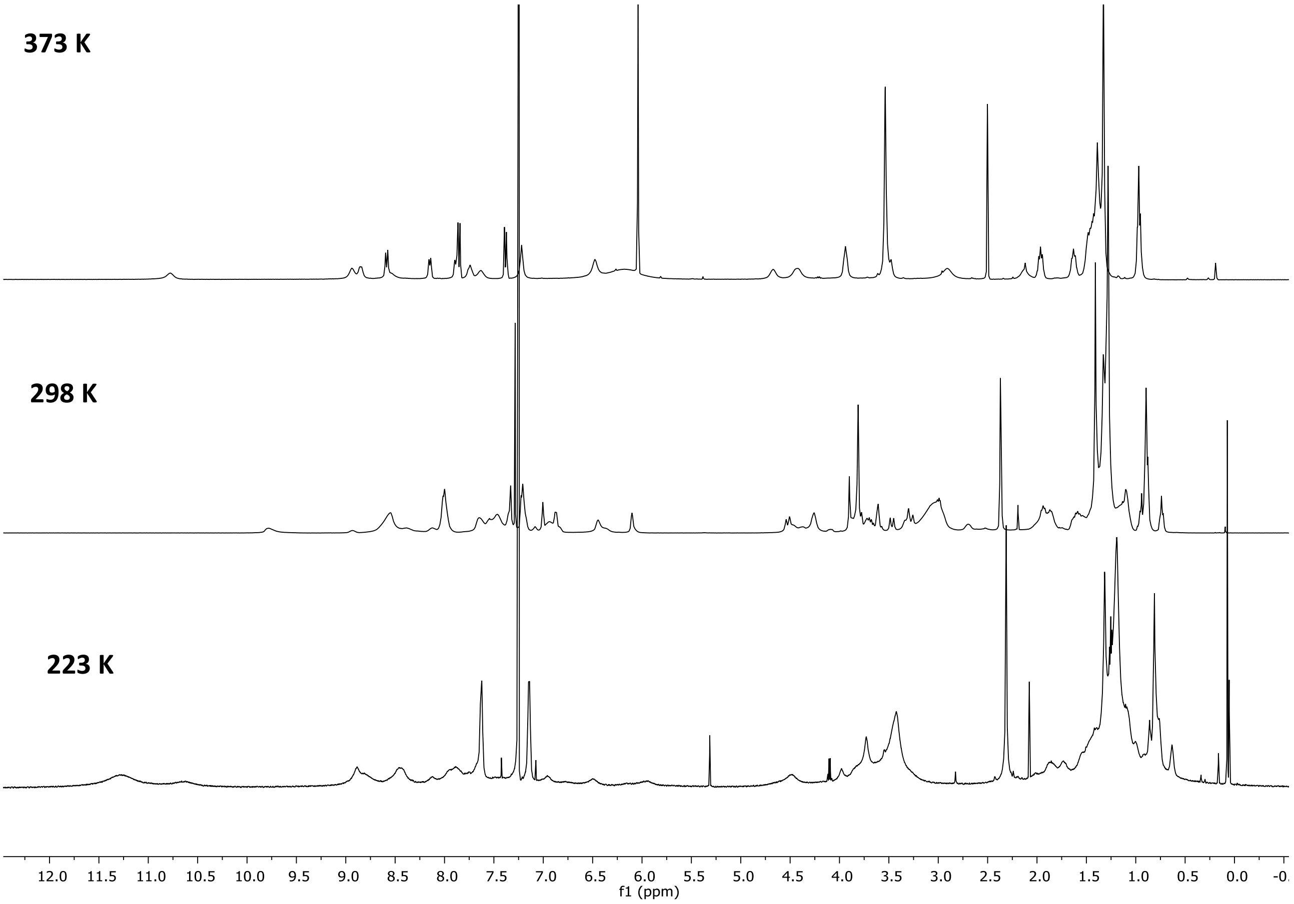

**Figure S18.** Stack plot of the $^1$H-NMR spectra of **TDA**(3H)3OTf at 373 K (1,1,2,2-tetrachloroethane-*d*$_2$, 400 MHz, top), at 298 K (CDCl$_3$, 400 MHz, middle) and 223 K (CD$_2$Cl$_2$, 600 MHz, bottom).

*Effect of the protonation on pseudorotaxane P[**TDA**(C)⊃DOV]2PF$_6$.*

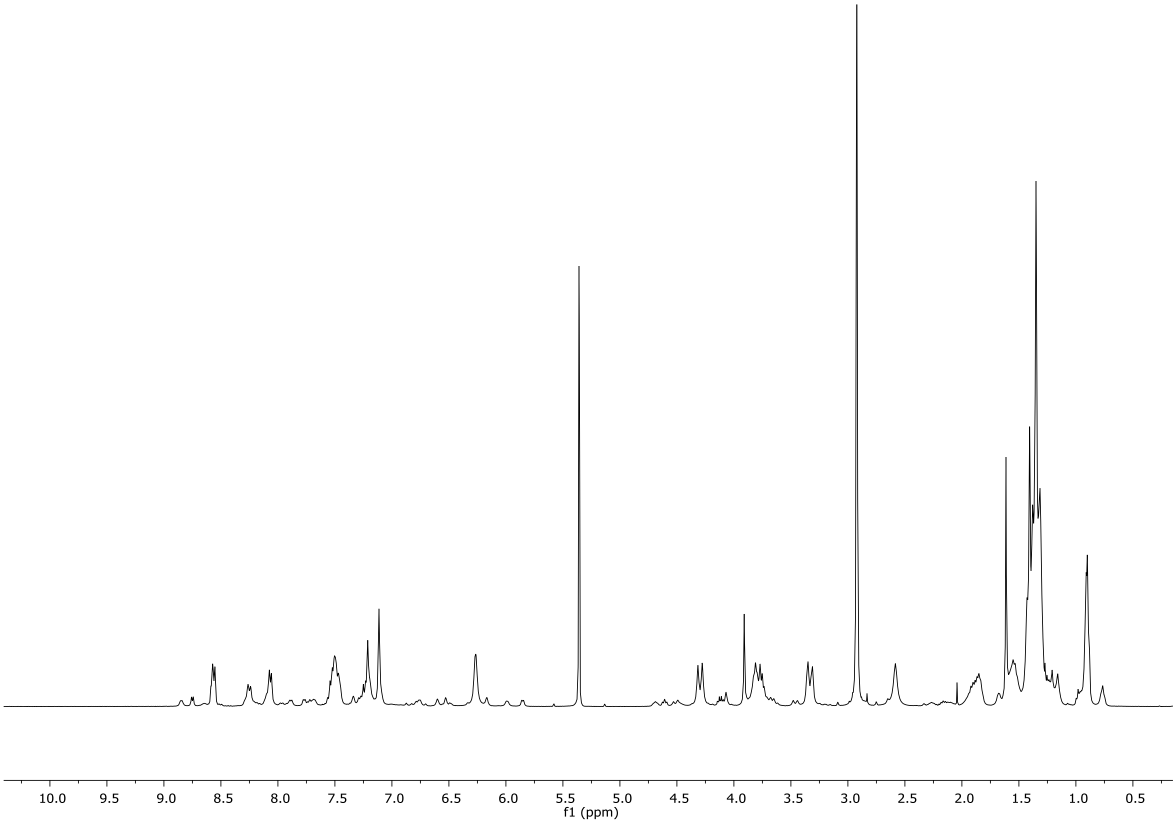

**Figure S19.** $^1$H-NMR ($CD_2Cl_2$, 400 MHz) spectrum of P[**TDA**(*C*)⊃DOV]2PF$_6$ (5 mM).

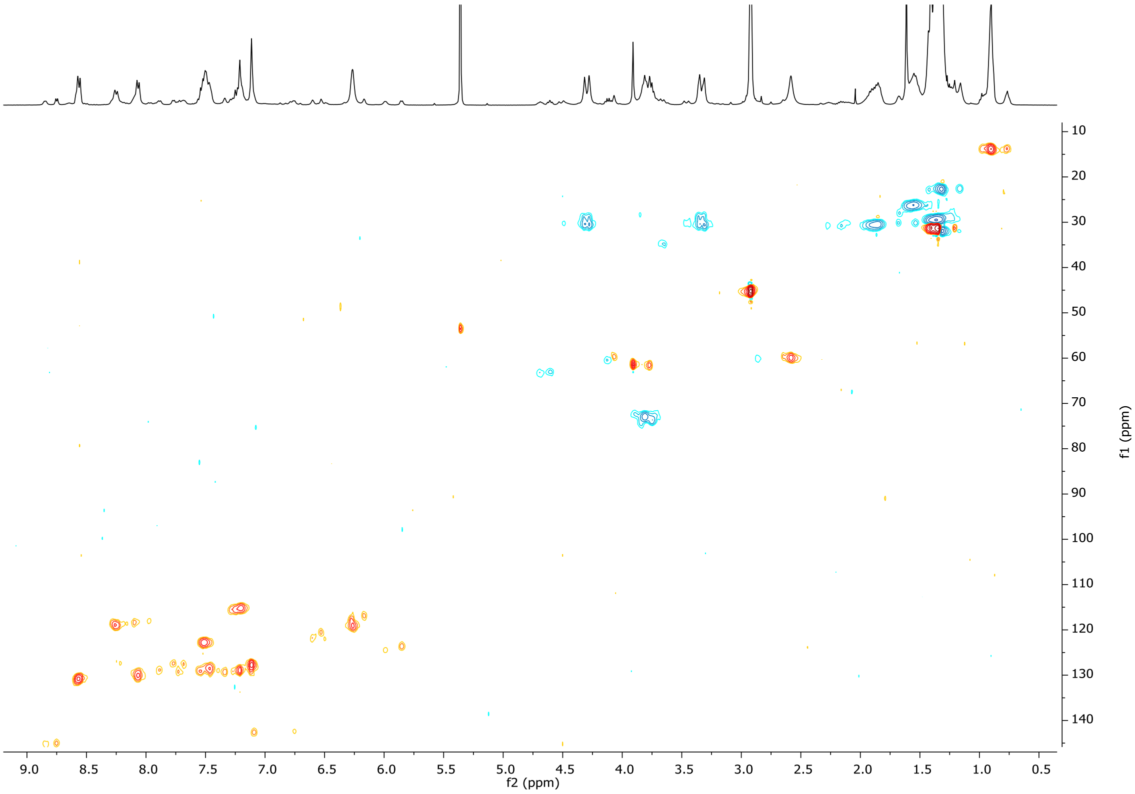

**Figure S20.** ge-2D multiplicity-edited ($CD_2Cl_2$, 400 MHz) NMR spectrum of P[**TDA**(*C*)⊃DOV]2PF$_6$. Red contours cross-peaks show $CH_3$, CH correlations while the blue contours show $CH_2$ correlations.

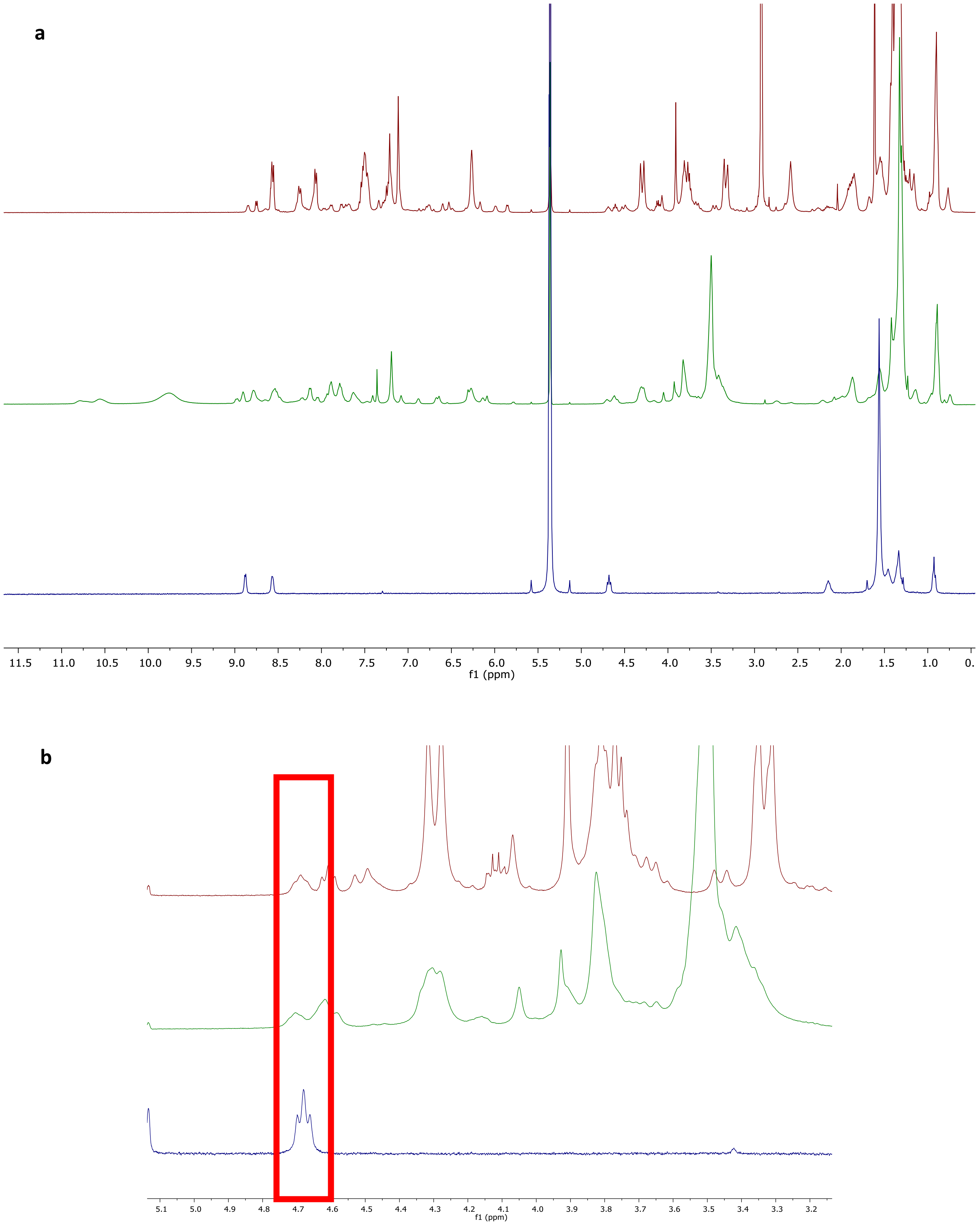

**Figure S21.** (**a**). Stack plot of the $^1$H-NMR spectra of P[**TDA**(*C*)⊃DOV]2PF$_6$ (top), P[**TDA**(3H)(*C*)⊃DOV]2PF$_6$(3OTf) (middle) and DOV•2PF$_6$ (298 K, CD$_2$Cl$_2$, 400 MHz, bottom); (b) detailed midfield region which compares the residual methylene CH$_2$ signals of threaded and free dioctylviologen axle.

- **Photophysical Characterisation of TDA**

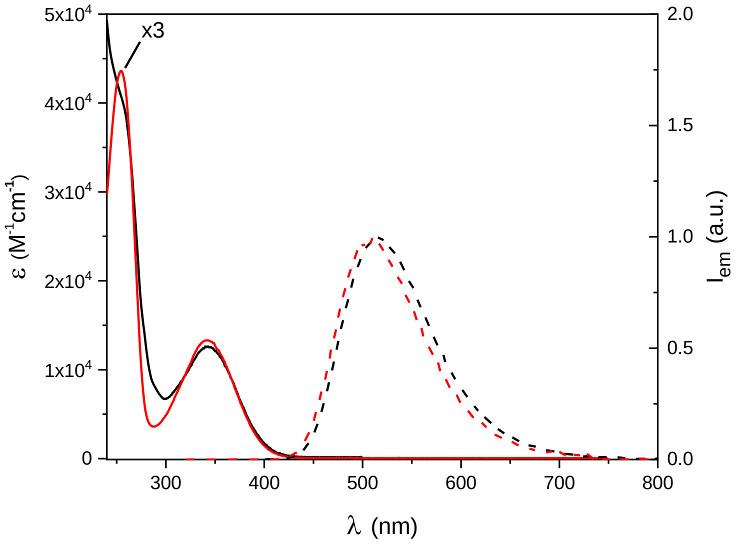

**Figure S22:** Absorption and emission spectra of **TDA** (solid and dashed black lines) and the dansyl amide model (solid and dashed red lines) in $CH_2Cl_2$ at room temperature. The absorption spectrum of dansyl amide is multiplied by a factor of 3 to simplify the comparison with the one of **TDA**.

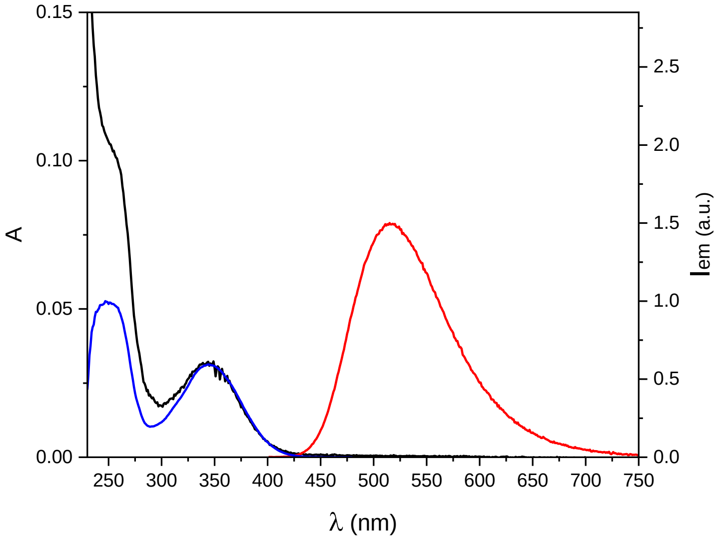

**Figure S23.** Absorption (black line), emission (red line, $\lambda_{ex}$=344 nm) and excitation (blue line, $\lambda_{em}$= 517 nm) spectra of a $CH_2Cl_2$ solution of **TDA** ($2.5 \times 10^{-6}$ M).

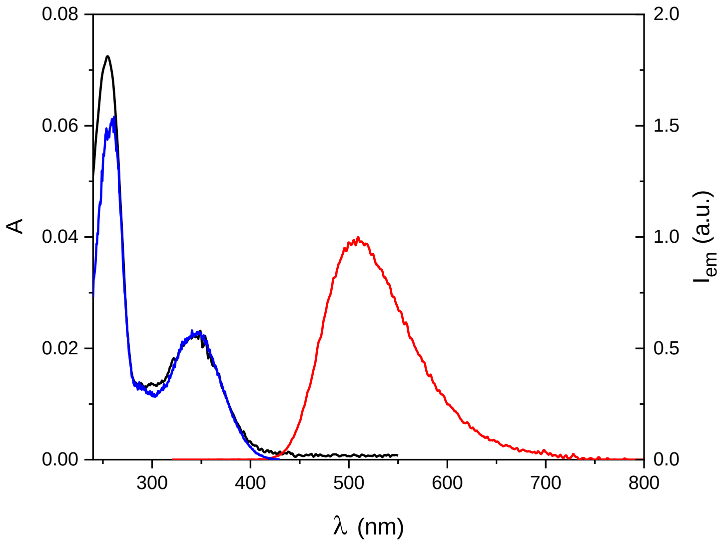

**Figure S24.** Absorption (black line), emission (red line, $\lambda_{ex}$=344 nm) and excitation (blue line, $\lambda_{em}$= 512 nm) spectra of a $CH_2Cl_2$ solution of dansyl amide (5.1 × $10^{-6}$ M).

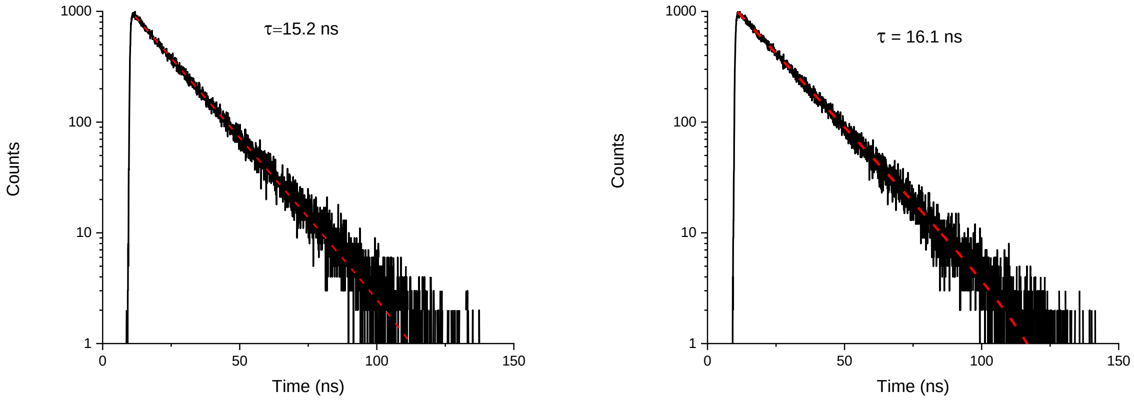

**Figure S25.** Fluorescence decay curve (black lines) of $CH_2Cl_2$ solutions of **TDA** (left, $\lambda_{em}$= 515 nm) and dansyl amide (right, $\lambda_{em}$= 512 nm). The red dashed lines represent the data fitting.

- **Protonation of TDA**

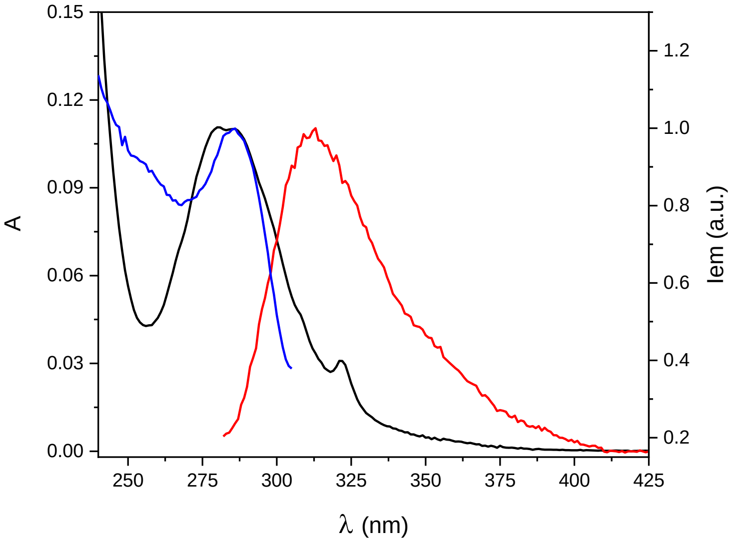

**Figure S26.** Absorption (black line), emission (red line, $\lambda_{ex}$= 255 nm) and excitation (blue line, $\lambda_{em}$= 350 nm) spectra of a $4.1 \times 10^{-6}$ M solution of protonated **TDA** in $CH_2Cl_2$.

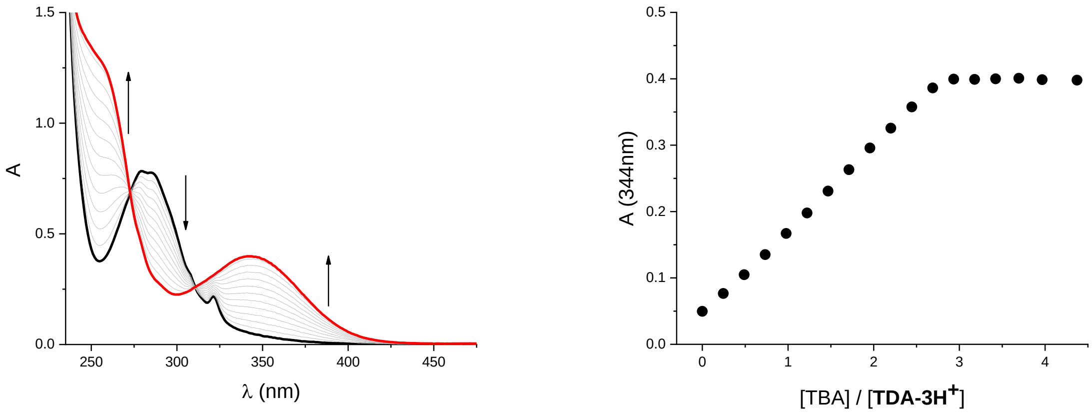

**Figure S27**. Left: Absorption spectra of a $CH_2Cl_2$ solution of protonated **TDA** ($3.3 \times 10^{-5}$ M) upon titration with tributylamine ($2.8 \times 10^{-3}$ M). Right: Absorption changes at 253 nm during the titration.

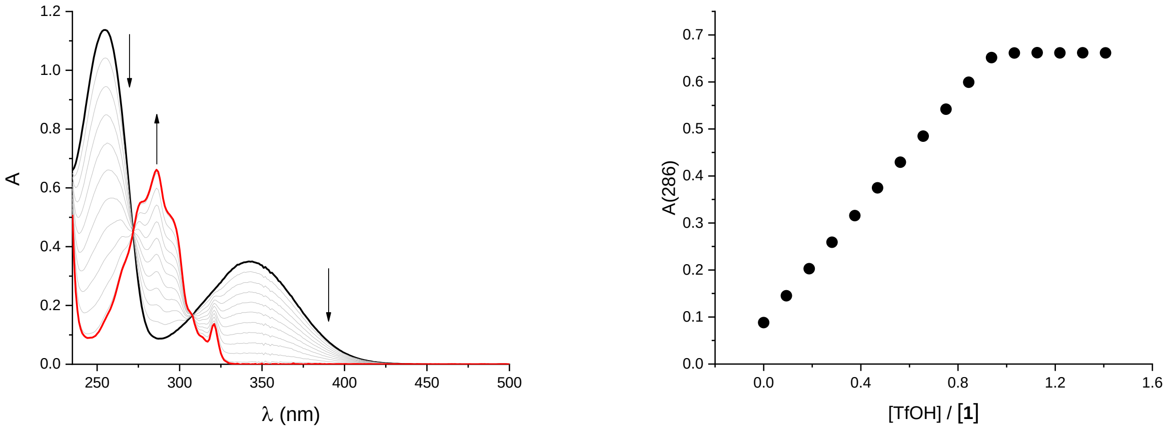

**Figure S28**. Left: Absorption spectra of a $CH_2Cl_2$ solution of dansyl amide **1** ($8.0 \times 10^{-5}$ M) upon titration with triflic acid ($1.1 \times 10^{-2}$ M). Right: Absorption changes at 253 nm during the titration.

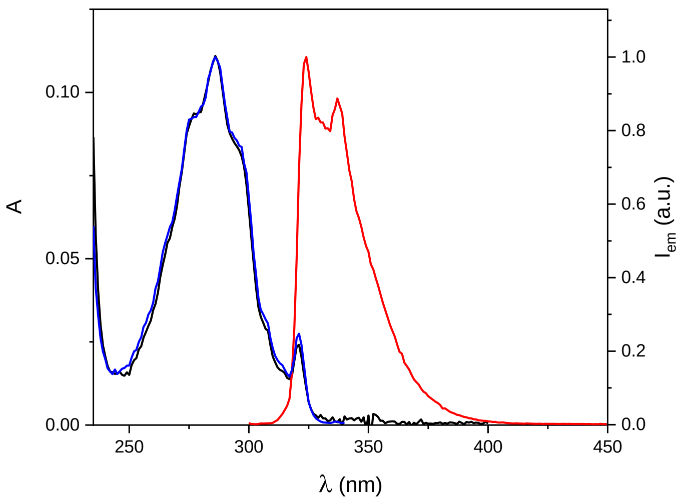

**Figure S29.** Absorption (black line), emission (red line, $\lambda_{ex}$=287 nm) and excitation (blue line, $\lambda_{em}$= 345 nm) spectra of a $CH_2Cl_2$ solution of protonated dansyl amide **1** ($1.4 \times 10^{-5}$ M, $\phi_{em}$= 0.07).

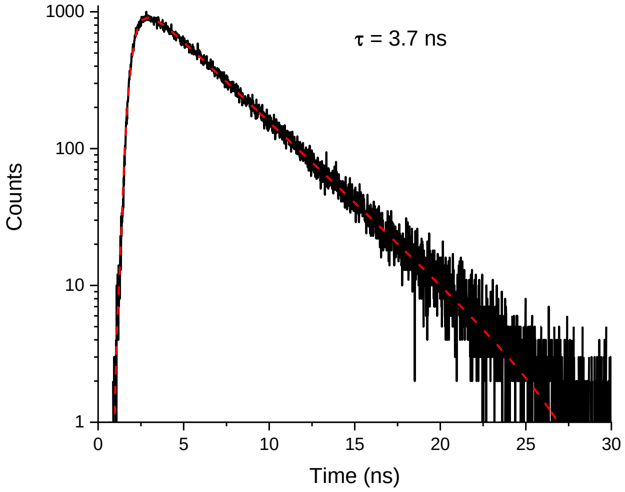

**Figure S30.** Fluorescence decay curve (black line) of a $CH_2Cl_2$ solution of protonated dansyl amide **1** ($\lambda_{em}$= 325 nm). The red dashed line represents the data fitting.

- **Association with DOV•2OTs**

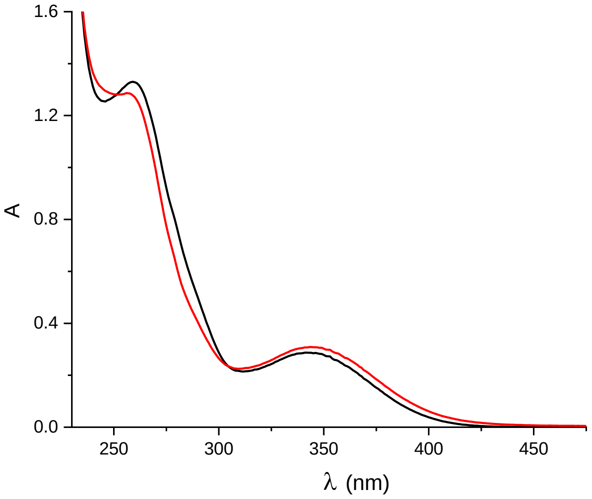

**Figure S31**. Sum of the absorption spectra (black line) and absorption spectrum of the mixture (red line) of $CH_2Cl_2$ solutions of **DOV**•2OTs (5.3 × $10^{-5}$ M) and **TDA** (5.7 × $10^{-5}$ M).

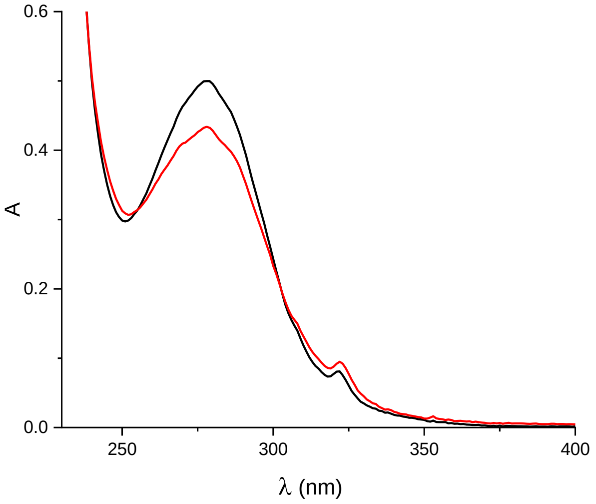

**Figure S32**. Sum of the absorption spectra (black line) and absorption spectrum of the mixture (red line) of $CH_2Cl_2$ solutions of **DOV•**2OTs ($4.0 \times 10^{-5}$ M) and protonated **TDA** ($2.9 \times 10^{-5}$ M).

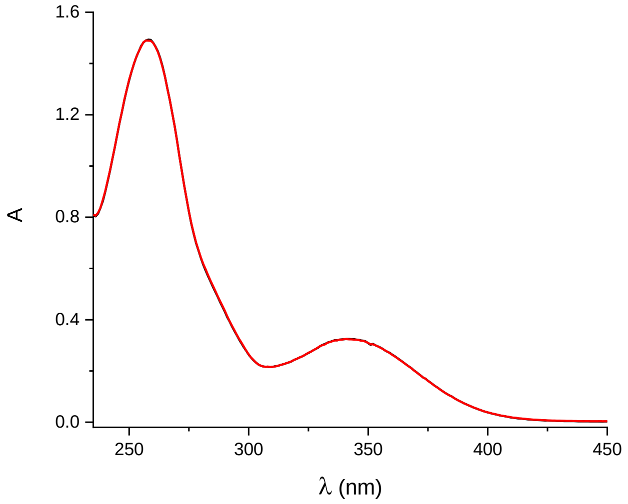

**Figure S33**. Sum of the absorption spectra (black line) and absorption spectrum of the mixture (red line) of $CH_2Cl_2$ solutions of **DOV•**2OTs ($5.7 \times 10^{-5}$ M) and dansyl amide **1** ($1.7 \times 10^{-4}$ M).

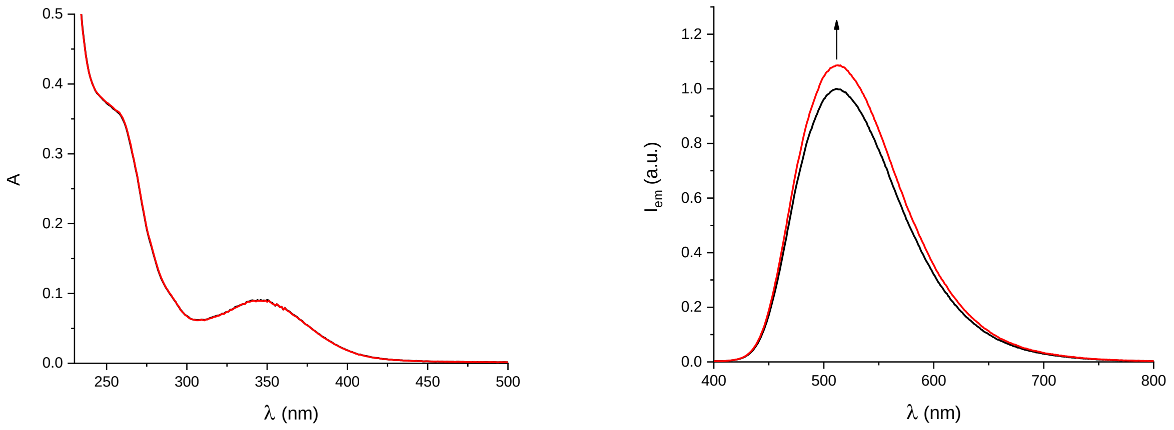

**Figure S34.** Absorption (left) and emission (right, $\lambda_{ex}$=343 nm) spectra of a $CH_2Cl_2$ solution of **TDA** (6.6 × $10^{-6}$ M) and **DOV•**2OTs (4.9 × $10^{-6}$ M) (black lines) upon addition of 3 equivalents of tetrabutylammonium triflate (red lines).

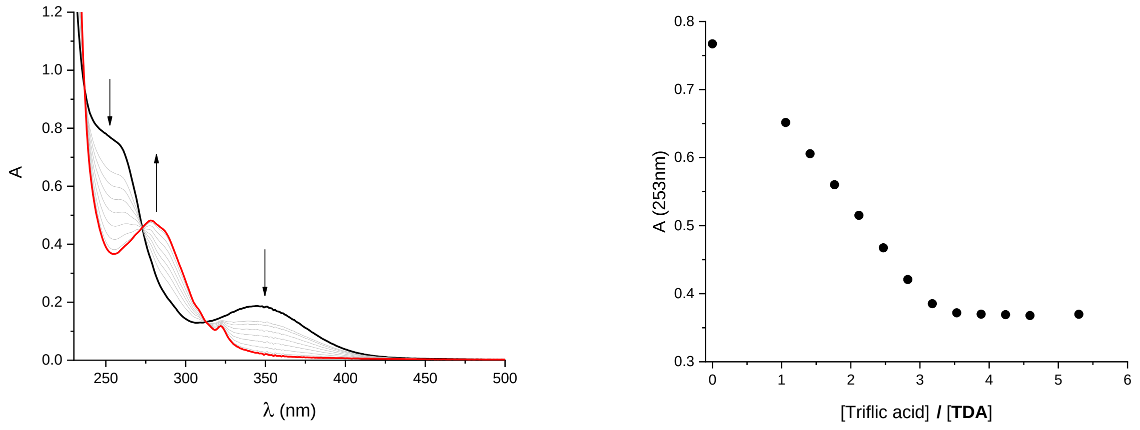

**Figure S35**. Left: Absorption spectra of a $CH_2Cl_2$ solution of **TDA** (1.7 × $10^{-5}$ M) and **DOV•**2OTs (1.6 × $10^{-5}$ M) upon titration with triflic acid (1.5 × $10^{-2}$ M). Right: Absorption changes at 253 nm during the titration.

- **Electrochemical Measurements**

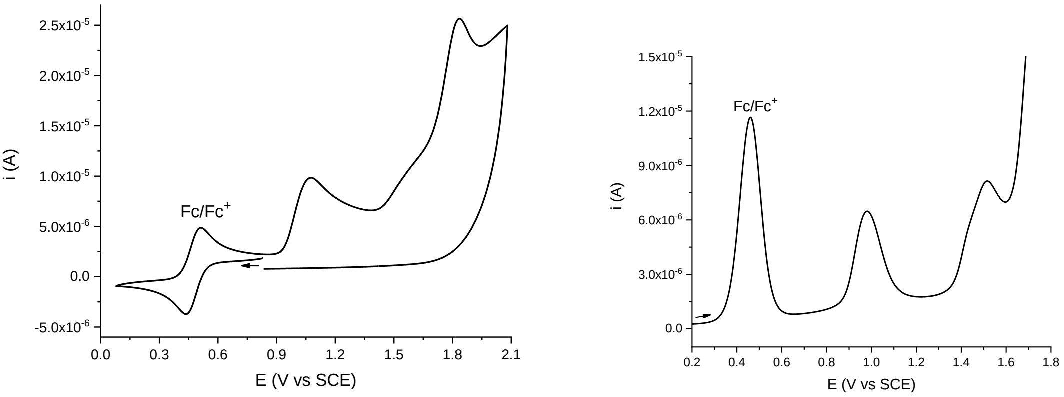

**Figure S36**. Cyclic voltammetry (left, scan rate: 100 mV/s) and differential pulse voltammetry (right, scan rate: 20 mV/s) of a $CH_2Cl_2$ solution of **TDA** ($2.5 \times 10^{-4}$ M) at room temperature. A 100-fold excess of $TBAPF_6$ was used as a supporting electrolyte.

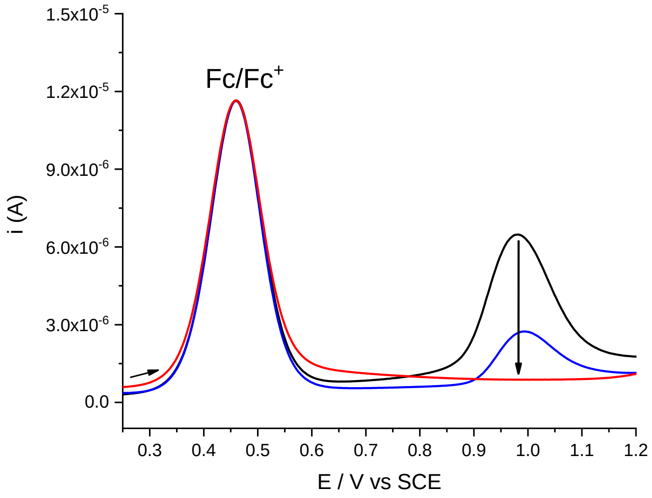

**Figure S37**. Differential pulse voltammetries (scan rate: 20 mV/s) of a $CH_2Cl_2$ solution of **TDA** ($2.5 \times 10^{-4}$ M) (black line) at room temperature upon addition of 3 equivalents (blue line) and 6.8 equivalents (red line) of triflic acid. A 100-fold excess of $TBAPF_6$ was used as supporting electrolyte. The oxidation process is related to the amine unit of the dansyl and it disappears upon protonation.

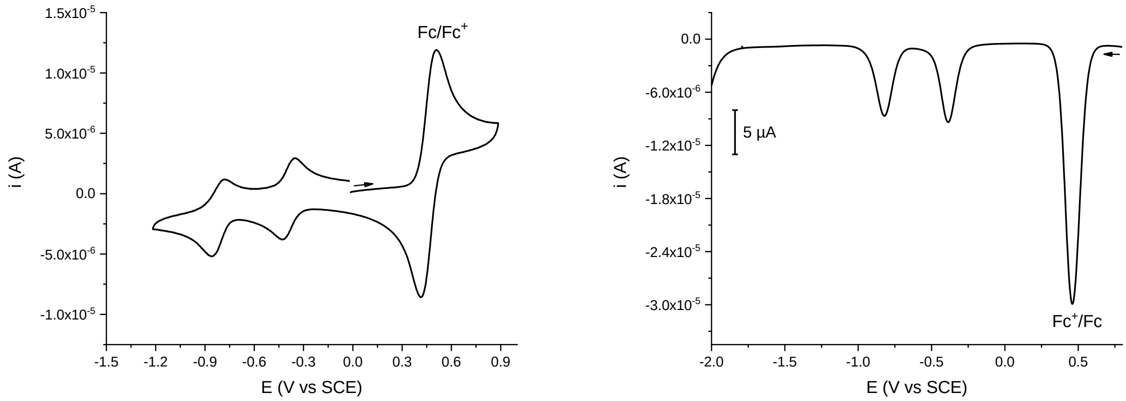

**Figure S38**. Cyclic voltammetry (left, scan rate: 200 mV/s) and differential pulse voltammetry (right, scan rate: 20 mV/s) of a $CH_2Cl_2$ solution of **DOV•**2OTs (1.0 × $10^{-4}$ M) at room temperature. A 100-fold excess of TBAOTs was used as supporting electrolyte.

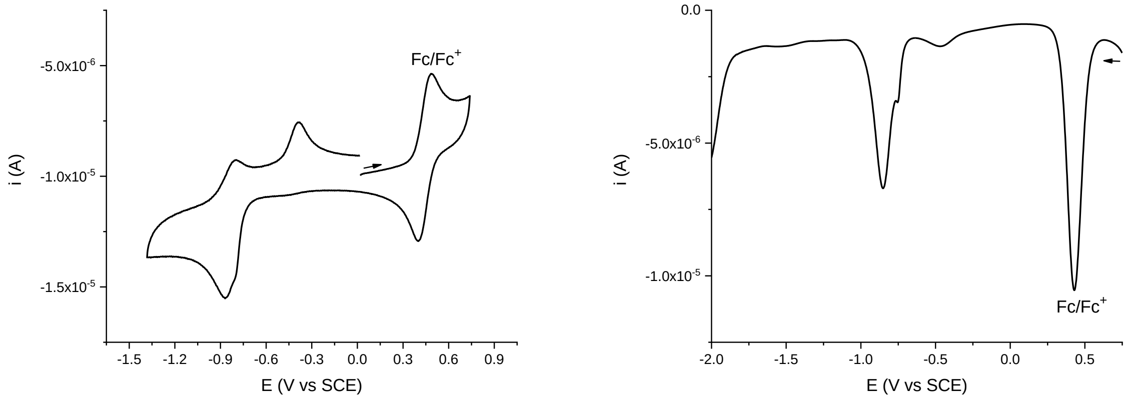

**Figure S39**. Cyclic voltammetry (left, scan rate: 200 mV/s) and differential pulse voltammetry (right, scan rate: 20 mV/s) of a $CH_2Cl_2$ solution of **DOV•**2OTs (8 × $10^{-5}$ M) and **TDA** (4.0 × $10^{-4}$ M) at room temperature. A 100-fold excess of TBAOTs was used as supporting electrolyte.

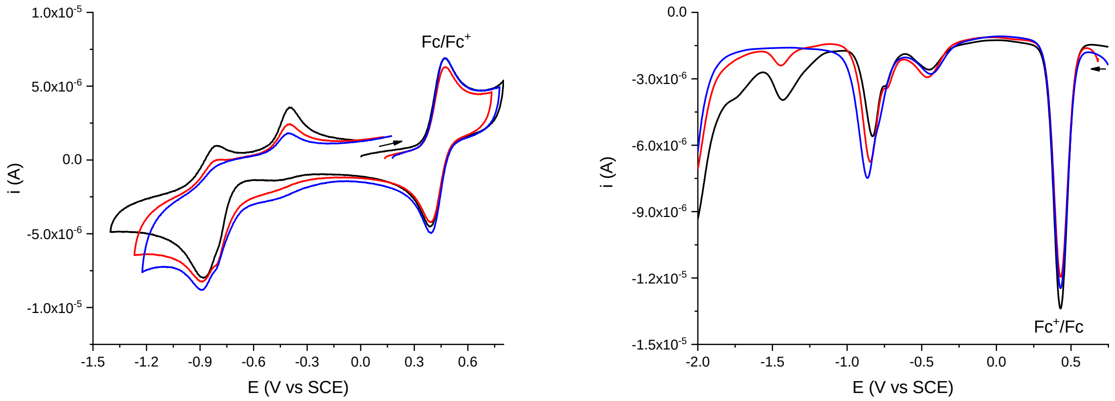

**Figure S40**. Cyclic voltammetry (left, scan rate: 200 mV/s) and differential pulse voltammetry (right, scan rate: 20 mV/s) of a $CH_2Cl_2$ solution of **DOV•**2OTs (2.0 × $10^{-5}$ M) and **TDA** (3.6 × $10^{-4}$ M) (black lines), and of the same solution after the addition of 1.5 (red lines) and 3.0 (blue lines) equivalents of triflic acid at room temperature. A 100-fold excess of TBAOTs was used as supporting electrolyte.

- **Kinetic Experiments**

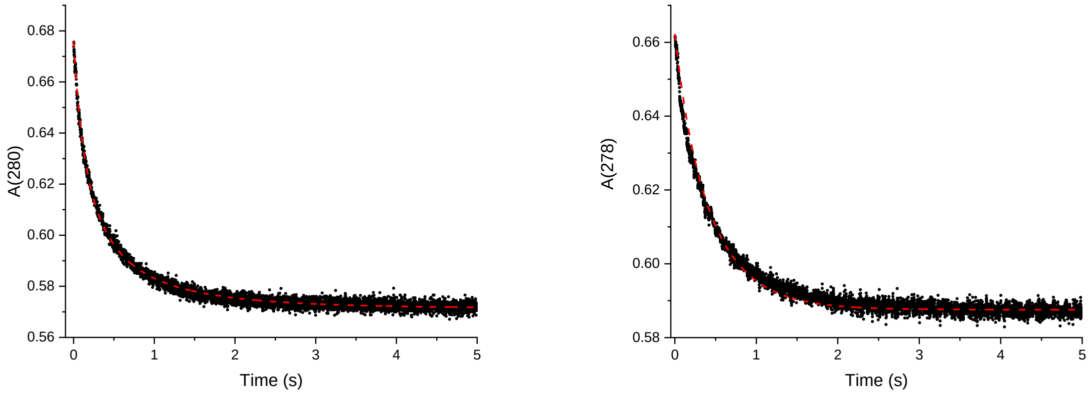

**Figure S41**. Time-dependent absorption changes recorded upon mixing in $CH_2Cl_2$ at 293 K: (left) **TDA** ($4.0 \times 10^{-5}$ M) and **DOV•**2OTs ($4.0 \times 10^{-5}$ M); (right) protonated **TDA** ($2.6 \times 10^{-5}$ M) and **DOV•**2OTs ($3.2 \times 10^{-5}$ M). The dashed lines represent the data fitting.

- **Photochemically-induced Dethreading**

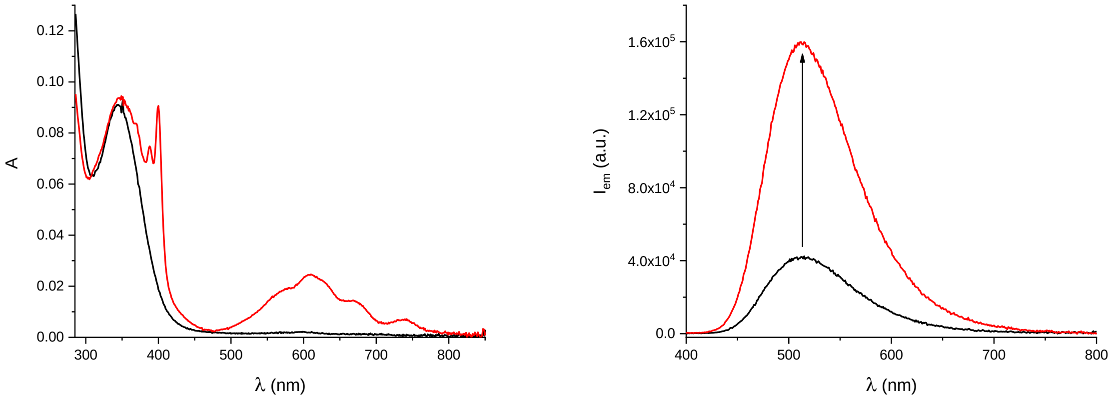

**Figure S42:** Absorption (left) and emission spectra (right, $\lambda_{ex}$=343 nm) of an argon-purged $CH_2Cl_2$ solution of **TDA** ($7.1 \times 10^{-6}$ M) and **DOV•**2OTs ($6.5 \times 10^{-6}$ M) (black lines) and of the same solution in the presence of Zn (red lines).

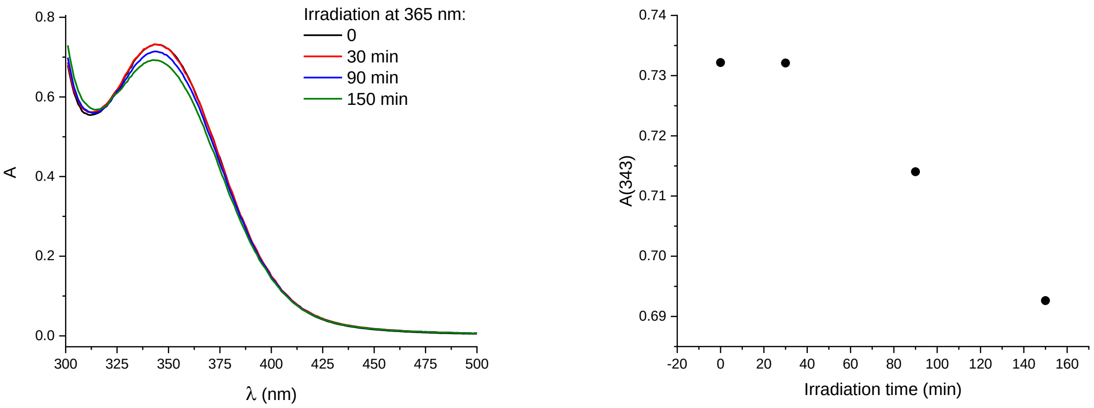

**Figure S43**. Left: Absorption spectra of an argon-purged $CH_2Cl_2$ solution of **TDA** ($6.5 \times 10^{-5}$ M) and **DOV•2OTs** ($6.5 \times 10^{-5}$ M) upon irradiation at 365 nm, up to 150 minutes. Right: Absorption changes at 343 nm during the irradiation. The small decrease of absorbance is probably related to the photobleaching of the dansyl unit.

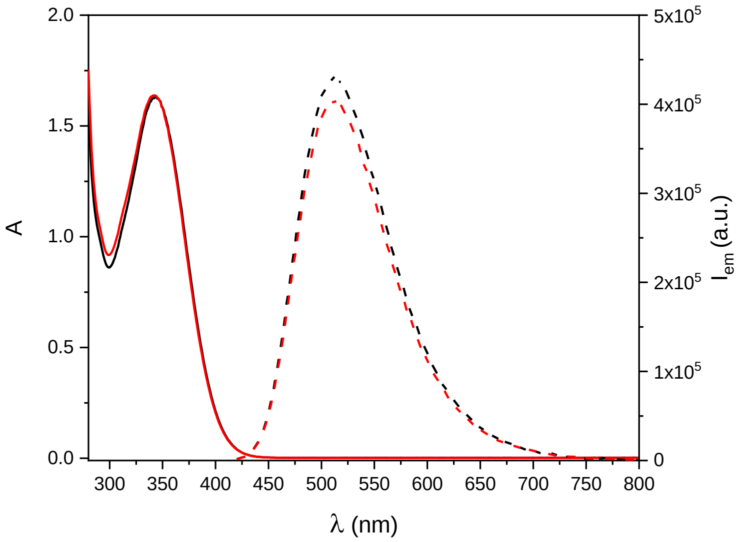

**Figure S44:** Absorption and emission spectra ($\lambda_{ex}$=410 nm) of an argon-purged $CH_2Cl_2$ solution of **TDA** ($1.3 \times 10^{-4}$ M) (solid and dashed black lines) and of the same solution in the presence of tributylamine (0.05 M) (full and dashed red lines).

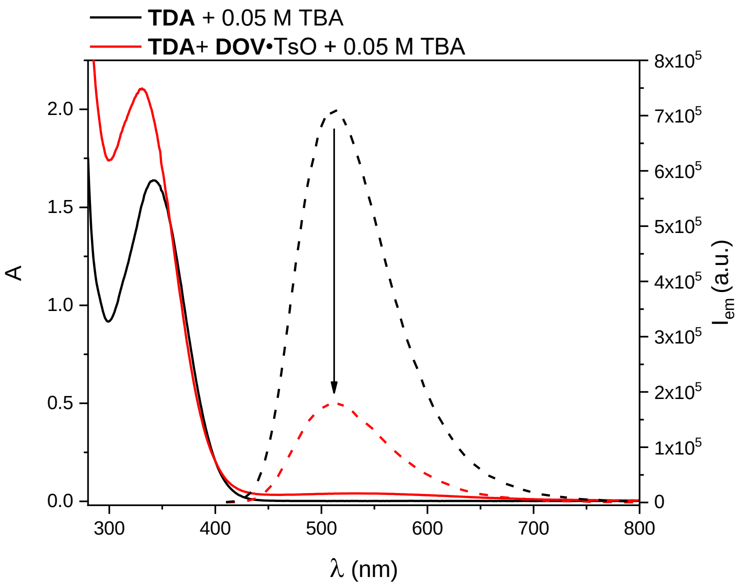

**Figure S45:** Absorption (full lines) and emission spectra (dashed lines, $\lambda_{ex}$=400 nm) of an argon-purged $CH_2Cl_2$ solution of **TDA** (1.3 × $10^{-4}$ M) and tributylamine (0.05 M) (black lines) and a solution of **TDA** (1.3 × $10^{-4}$ M), **DOV•**2OTs (2.0 × $10^{-4}$ M) and tributylamine (0.05 M) (red lines).

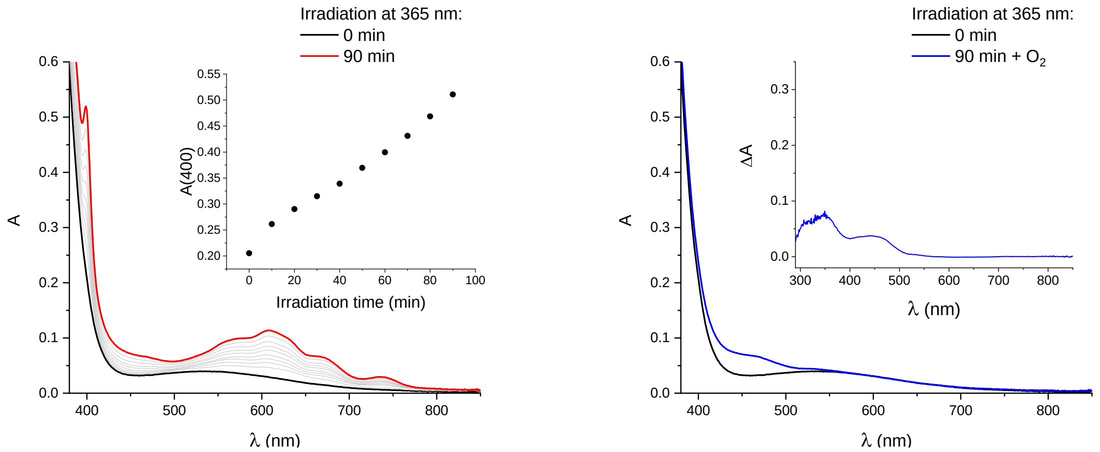

**Figure S46**. Left: Absorption spectra of an argon-purged $CH_2Cl_2$ solution of **TDA** (1.3 × $10^{-4}$ M), **DOV•**2OTs (2.0 × $10^{-4}$ M) and tributylamine (0.05 M) upon irradiation at 365 nm, up to 90 minutes. Inset: Absorption changes at 400 nm during the irradiation. Right: Absorption spectra before the irradiation (black line) and after the irradiation and subsequent addition of oxygen (blue line). Inset: Difference of the two spectra shown in the graph.

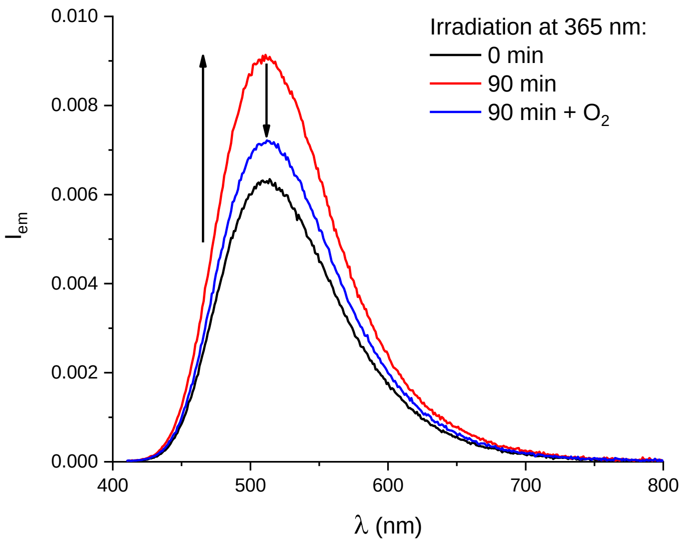

**Figure S47**. Emission spectra ($\lambda_{ex}$=400 nm) of an argon-purged $CH_2Cl_2$ solution of **TDA** ($1.3 \times 10^{-4}$ M), **DOV•**2OTs ($2.0 \times 10^{-4}$ M) and tributylamine (0.05 M) before irradiation (black line), after 90 minutes of irradiation at 365 nm (red line) and subsequent addition of oxygen (blue line). The emission spectra were corrected with the calibration curve of the spectrofluorimeter[1] in order to have a linear relationship between $I_{em}$ and the concentration of the fluorophore. The increase of emission upon irradiation allows to estimate that around 10% of the complex is dissociated.

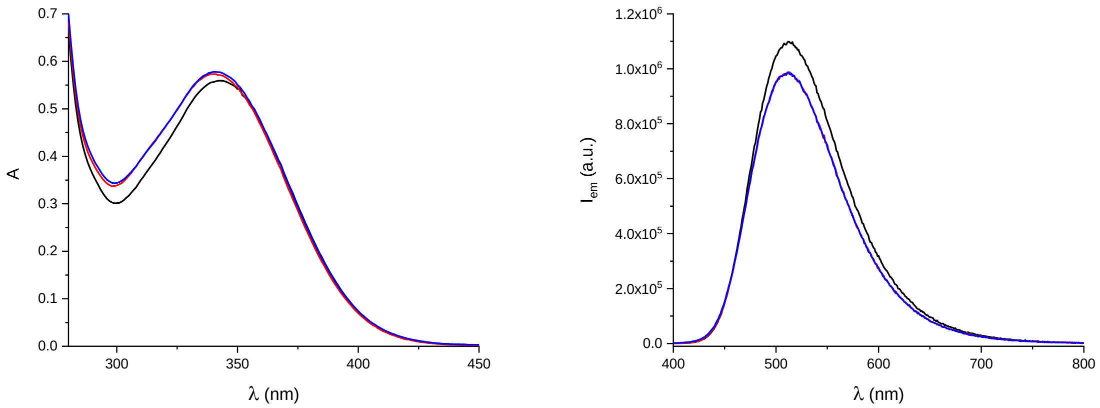

**Figure S48**. Left: Absorption (left) and emission (right, $\lambda_{ex}$=343 nm) spectra of an argon-purged $CH_2Cl_2$ solution of **TDA** ($4.4 \times 10^{-5}$ M) and tributylamine (0.05 M) (black lines), and of the same solution after 160 minutes (red lines), and after 90 minutes of irradiation at 365 nm (blue lines).

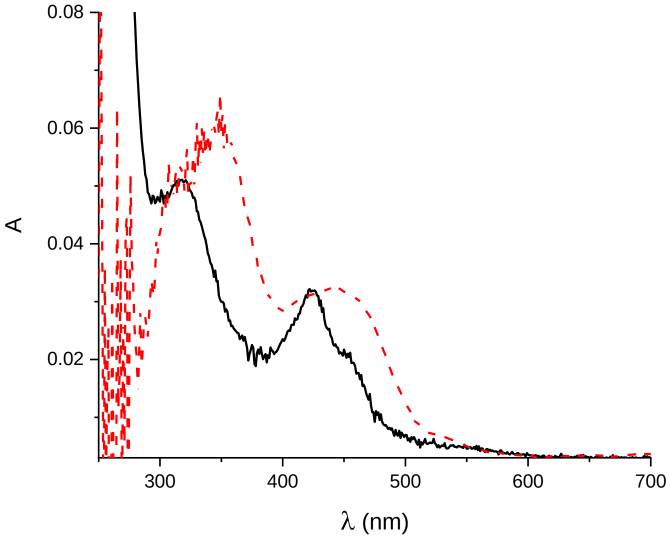

**Figure S49.** Spectroelectrochemistry (black line) of an argon-purged $CH_2Cl_2$ solution of tributylamine (0.01 M) in presence of $TBAPF_6$ (0.1 M) ($E_{appl}$= +1.5V). The difference spectrum taken from the irradiation experiment of Figure S46 is reported for comparison (red dashed line). The similarity between the two spectra suggests that the band observed upon irradiation of **TDA⊃DOV** is related to an oxidation product of the tributylamine.

## Notes and References

[1] A. Credi and L. Prodi, *J. Mol. Struct.,* 2014, *1077*, 30–39